EXPERIMENTAL INVESTIGATION OF FILTRATION EFFICIENCY AND PRESSURE DROP BEHAVIOR OF HIGH POROSITY GASOLINE PARTICULATE FILTERS

A Thesis

by

QUINTON JAMES PORTER

Submitted to the Office of Graduate and Professional Studies of
Texas A&M University
in partial fulfillment of the requirements for the degree of

MASTER OF SCIENCE

Chair of Committee,	Andrea Strzelec
Committee members,	Jaime Grunlan
	David Staack
Head of Department,	Andreas Polycarpou

May 2018

Major Subject: Mechanical Engineering

ABSTRACT

The increasing number of gasoline direct injection (GDI) vehicles on the roads has drawn attention to their particulate matter (PM) emissions, which are greater both in number and mass than port fuel injected (PFI) spark ignition (SI) engines. Regulations have been proposed and implemented to reduce exposure to PM, which has been shown to have negative impacts on both human health and the environment. Currently, the gasoline particulate filter (GPF) is the proposed method of reducing the amount of PM from vehicle exhaust, but modifications to improve the filtration efficiency (FE) and reduce the pressure drop across the filter are yet needed for implementation of this solution in on-road vehicles. This work evaluates the increase to FE, while keeping the backpressure penalty at a minimum, for GPF samples with different wall thicknesses and cell densities. For both unmodified and modified GPFs, the filtration efficiency was studied using a scanning mobility particle sizer (SMPS), and the pressure drop across the filter was obtained using a differential pressure transducer. The performance of the unmodified GPFs was investigated at three space velocities: 15,000 hr^{-1}, 30,000 hr^{-1}, and 60,000 hr^{-1}. Increasing space velocity through unmodified GPFs results in decreasing FE by approximately 5% for every 15,000 hr^{-1} increase, meaning a GPF has its lowest FE and highest pressure drop at 60,000 hr^{-1}. The GPF with the lowest initial FE and pressure drop, 300-10, was modified by preloading calcium sulfate ($CaSO_4$) to form a cake layer on the walls. An improvement of about 10% to the filtration efficiency and increase of about 6% to the pressure drop was measured for a GPF loaded to 20 $\frac{g}{L}$. This indicates that a preloaded cake layer can improve performance with less penalty than increasing wall thickness.

CONTRIBUTORS AND FUNDING SOURCES

Contributors

This work was supervised by a thesis committee consisting of Professor Andrea Strzelec and David Staack of the Department of Mechanical Engineering and Professor Jaime Grunlan of the Material Science Department.

All work for the thesis was completed by the student, under the advisement of Dr. Andrea Strzelec of the Department of Mechanical Engineering.

Funding Sources

Graduate study was supported by a fellowship from Texas A&M University and a Graduate assistanceship from the Department of Mechanical Engineering under Dr. Strzelec.

TABLE OF CONTENTS

Page

LIST OF FIGURES

Page

LIST OF TABLES

Page

NOMENCLATURE

$CaSO_4$ – Calcium Sulfate

CPC – Condensation Particle Counter

CPSI – Cells per Square Inch

DMA – Differential Mobility Analyzer

DPF – Diesel Particulate Filter

EPA – Environmental Protection Agency

GDI – Gasoline Direct Injection

GPF – Gasoline Particulate Filter

HDV – Heavy Duty Vehicles

LDV – Light Duty Vehicles

MFC – Mass Flow Controller

PFI – Port Fuel Injection

PM – Particulate Matter

PN – Particulate Number

SiC – Silicon Carbide

SMPS – Scanning Mobility Particle Sizer

CHAPTER I

INTRODUCTION AND LITERATURE REVIEW

Government agencies across the world work diligently to define regulations for air quality. Maintaining high air quality remains a priority of the United States Environmental Protection Agency (US EPA) as proven by the amendments and additions to the Clean Air Act of 1970 (CAA), which was the first federal attempt by the United States to protect the public from hazardous air pollutants [1, 2]. One of the largest sources of air pollution is vehicle exhaust emissions, which include many gaseous species as well as particulate matter (PM).

Unlike the gaseous emissions found in vehicle exhaust, PM is uniquely categorized by physical form: discrete liquid or solid particles within the air ranging from approximately 5.0 nm - 0.1 mm in diameter [2]. Particles with diameters below 100 nm, have been shown to have greater toxicity within the human body despite no difference in chemical composition from larger particles [3]. Further, epidemiological studies have shown that inhalation of particles under 100 nm can cause cancer and increase the incidences of cardiovascular and respiratory diseases, which can result in challenged breathing, irregular heartbeat, and even premature death [4-8]. In fact, it is believed that PM contributes to an estimated 800,000 annual fatalities [4].

In addition, there are deleterious environmental effects associated with PM. Fine particles below 1 μm, like those in exhaust, can remain in the air for weeks and travel great distances in the wind; whereas gravitational forces move larger particles to the ground more quickly [3]. Haze from fine particles suspended in the air causes reduced visibility, and deposited particulates have increased the acidity of water, changed the nutrient balance in soil, and generally negatively impacted the diversity of ecosystems [6, 9]. Reduction of black carbon

emissions, which PM envelopes, has been presented as one of the fastest ways to slow global warming [10]. The atmospheric temperature increase associated with global warming is thought to be caused by the trapping of thermal energy due to the changing emissivity caused by particulate deposits, especially at the polar ice caps.

Recognizing the undesired health and environmental effects from exposure to PM, regulators across the globe have been reducing the allowable PM emissions from vehicles powered by internal combustion engines (ICEs). In the United States, EPA Tier 3 regulatory standards focus on particulate mass, and limit the emissions of vehicles to 30 $\frac{\text{mg}}{\text{mile}}$ [8, 11]. Standards on a mass basis require larger diameter particles to be collected but allow for small diameter PM to be emitted into the atmosphere, since they contribute very little to the total particulate mass in the exhaust. European standards focus instead on particle number (PN) emissions. In 2011, the European Commission set a number limit for PM emissions for particulate greater than 23 nm in diameter [8]. This size cutoff was not chosen based on health effects, since it is known that the smaller particles pose a greater risk, but rather due to the poor reliability of the measurement equipment below 23 nm. The implementation of the PM limit in the Euro 5b standard expanded the focus to include gasoline vehicles, instead of only diesel. Specifically, gasoline direct injection (GDI) vehicles will be under scrutiny, with the PN standards in the Euro 6 regulation [12]. It is believed that the implementation of the European standards of 4.5 $\frac{\text{mg}}{\text{km}}$ with $6 * 10^{11}$ $\frac{\#}{\text{km}}$ of PM will lead to the development of similar standards in the U.S. By 2025, GDI vehicles in Europe and likely, the U.S. shortly thereafter, will have to comply with the same stringent standards as diesel [13, 14]. Since the Euro 4 in 2005, aggressive reductions for allowable PM (illustrated in grey) have been proposed, as shown in **Figure 1(a)**. The allowable

mass emitted in vehicle exhaust was reduced from 250 $\frac{mg}{km}$ by 75 % in the U.S. Tier 2 and 92 % for U.S. Tier 3, which is circled in blue. The dates for the PN limit implementation and the phase-in of the more stringent mass limits are shown in **Figure 1(b)**. These continuous reductions create a significant challenge for automotive engineers to remain in compliance with regulatory standards.

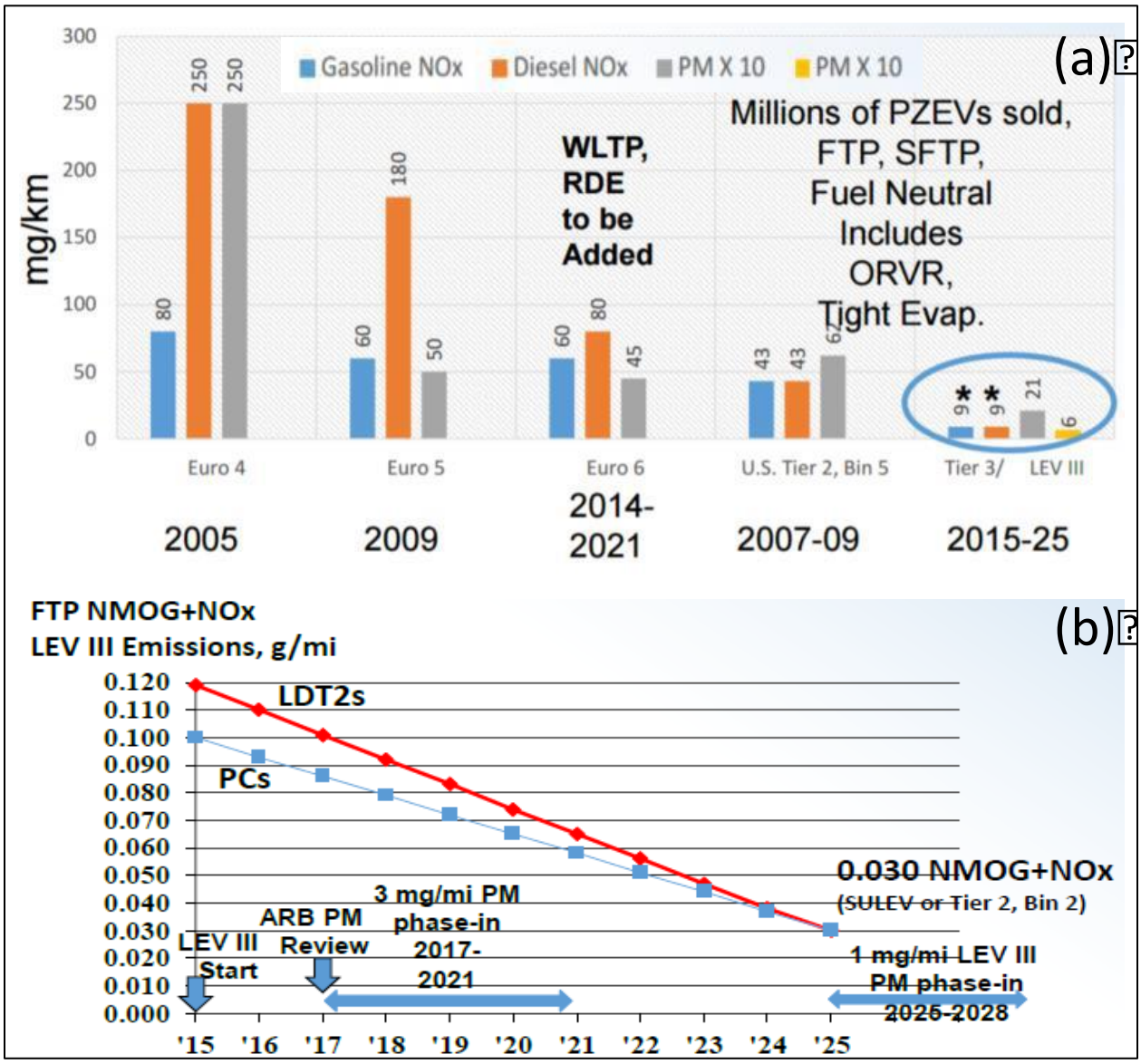

Figure 1 (a) Proposed standards for reducing emissions in the United States and Europe from 2005 to 2025 [14]. Note that US Tier 2, Bin 5 is the equivalent to ARB LEV III. (b) Phase in plan for the LEV III/ Tier 3 standards with decreasing PN emissions for GDI vehicles. Adapted from [13].

1.1 Particulates from Gasoline Direct Injection Engines

Recent advancements in GDI technology have increased fuel efficiency over port fuel injection (PFI) engines resulting in a reduction of CO_2 emissions, which has led to an increasing presence of GDI vehicles in the market place [12, 15]. It is estimated that 33 million GDI powered vehicles will be on the road by 2020, as depicted by the trend in **Figure 2** [16].

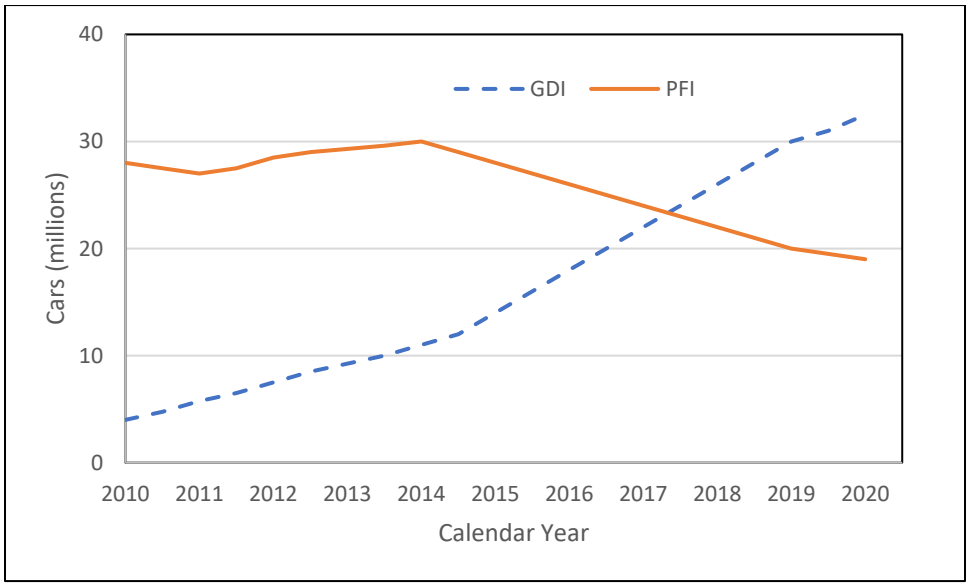

Figure 2: Projected global trend for increasing number of GDI vehicles on the road compared to port fuel injection (PFI) adapted from Craig. Adapted from [16].

In GDI engines, the fuel is directly injected into the cylinder, near the spark plug, instead of being pre-mixed with air in the intake manifold as is done in port fuel injection engines. For GDI engines, the stratified fuel-air mixture is combustible despite the overall mixture being too lean for combustion in a homogenous mixture. This results in better fuel efficiency, similar to lean-burn diesel engines, but more PM formation than PFI engines [8]. The increase toward

diesel-like fuel efficiency has also resulted in PM emissions that approach the size and number of their diesel counterparts, as exhibited in **Figure 3** and **Figure 4** [8, 17-19].

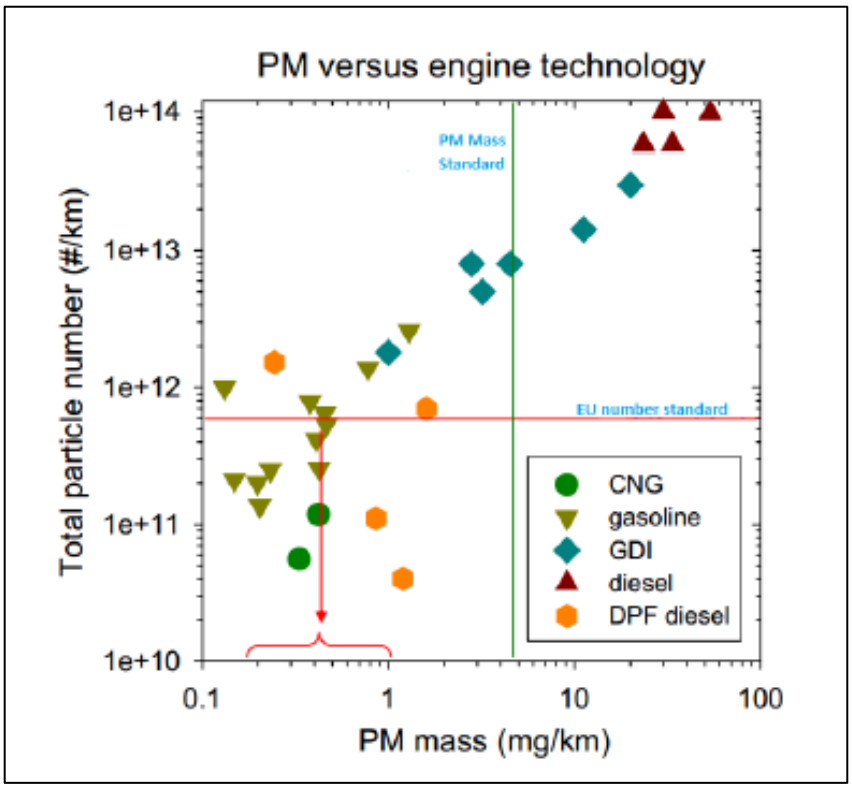

Figure 3: Particle number and particulate mass emissions for GDI, PFI and diesel engines. Trend of higher PN and PM mass for GDI over PFI is evident with blue diamonds above the lines representing the number standard and mass standard. Adapted from [8].

Further, **Figure 4** shows that the PM emissions are not only higher for GDI than PFI for both stoichiometric and lean operation, but they also exceed the proposed future limits for vehicles [15]. The gasoline engines in **Figure 3** and the MPFI of **Figure 4** are synonymous and operate under stoichiometric conditions.

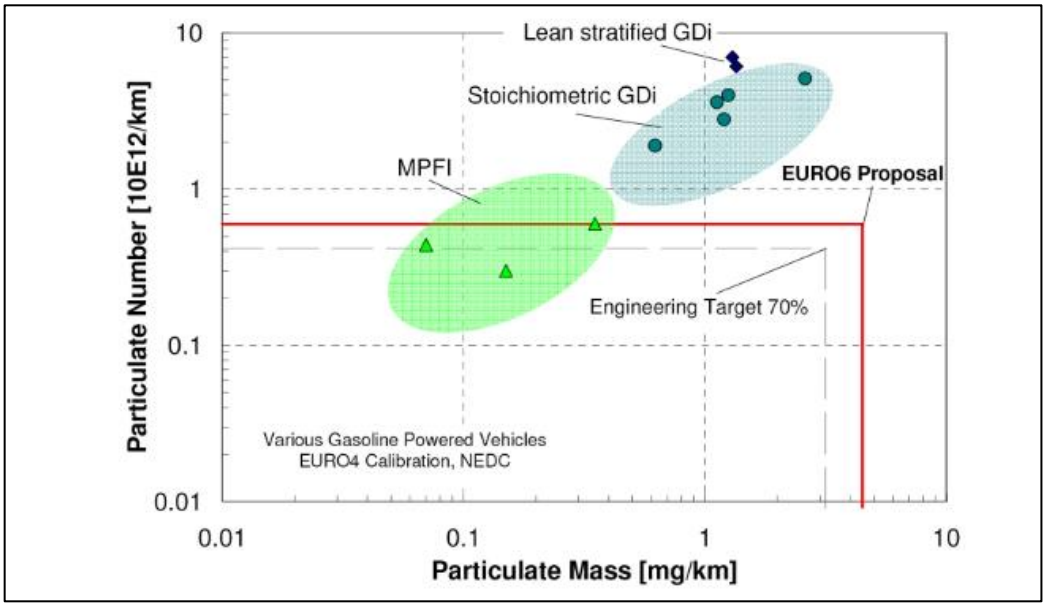

Figure 4: GDI and PFI PM emissions compared to the EURO 6 standard showing that GDI engines exceed the proposed limit. Adapted from [11].

1.2 Particulate Filters

Since 2003, regulatory standards have required diesel vehicles to use diesel particulate filters (DPFs) to capture PM emissions. Currently, DPFs are considered to be the only feasible aftertreatment technology capable of reducing the PM emissions to meet the standards [20]. The particulate filter is a wall-flow monolith, which mechanically removes PM from flowing gas as illustrated in **Figure 5.** Cordierite and silicon carbide (SiC) are two common and cost-effective materials that are used [20-22]. Wall-flow monoliths typically consist of porous walls in a honeycomb structure. The faces consist of alternating channels that are plugged on one end and open on the other. An open channel on the inlet face is surrounded by neighboring channels that are closed on the inlet but open on the opposite end. Particle laden exhaust gas flows into the unplugged inlet channel and is forced to traverse through the porous walls to enter adjacent

channels and flow through the outlet. Particulates are unable to pass through the pores and remain in the filter.

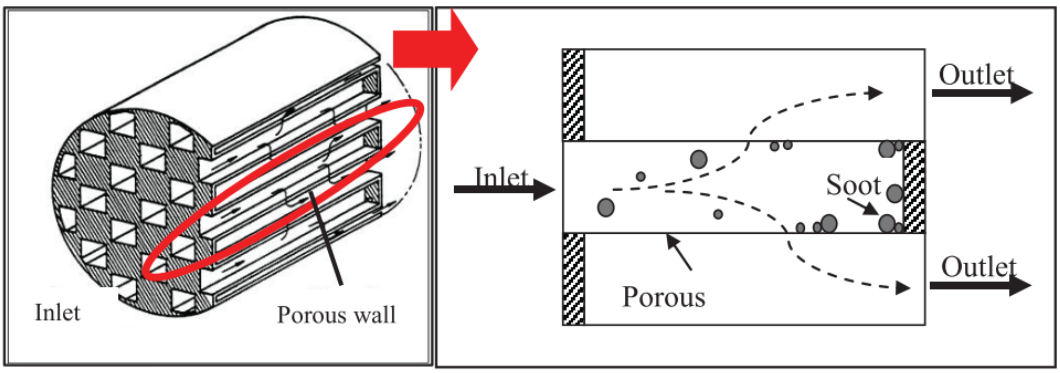

Figure 5: Depiction of a wall-flow monolith and the mechanical removal PM from exhaust. Exhaust gas with a high concentration of PM flows into the channels open on the inlet face but closed on the opposite end. The gas flows through the porous walls and is separated from particulate. The gas exits through the outlet with a much lower concentration of PM. Adapted from [23].

For operational efficiency and regulatory compliance, particulate filters need to meet several requirements: high efficiency, low back pressure through the lifetime of the filter, corrosion and erosion resistance, and high thermal stability [24]. Previous research on DPFs indicates that SiC and cordierite are durable and maintain their structural integrity during use [20]. To meet the regulatory standards and reduce the PN emissions of current vehicles to $6*10^{11}$ $\frac{\#}{\text{km}}$, a filtration efficiency between 94% and 99% must be achieved, as shown in **Table 1**. Reducing the backpressure penalty remains a concern [20, 22].

Table 1: Filtration efficiency required to abate the number of particles required to meet standard Euro 6b for a range of GDI vehicle PM emissions.

PM Emitted ($1*10^{13}$ $\frac{\#}{\mathrm{km}}$)	1.0	2.0	3.0	4.0	5.0	6.0	7.0	8.0
Required Filtration Efficiency (%)	94.0	97.0	98.0	98.5	98.8	99.0	99.1	99.3

Though the filtration efficiency of clean DPFs is only around 60%, they quickly reach greater than 95% efficiency due to the formation of a soot cake on the wall of the substrate, which captures many other particles [20, 25]. The soot cake forms quickly during operation, building up on the porous wall as shown in **Figure 6,** and increases filtration efficiency by decreasing the porosity of the filter [3, 23, 24, 26]. In the bottom, right picture **(d)**, the reduced porosity on the substrate surface is evident. Less particulate can pass through the soot cake than the courser substrate beneath, resulting in higher filtration efficiency.

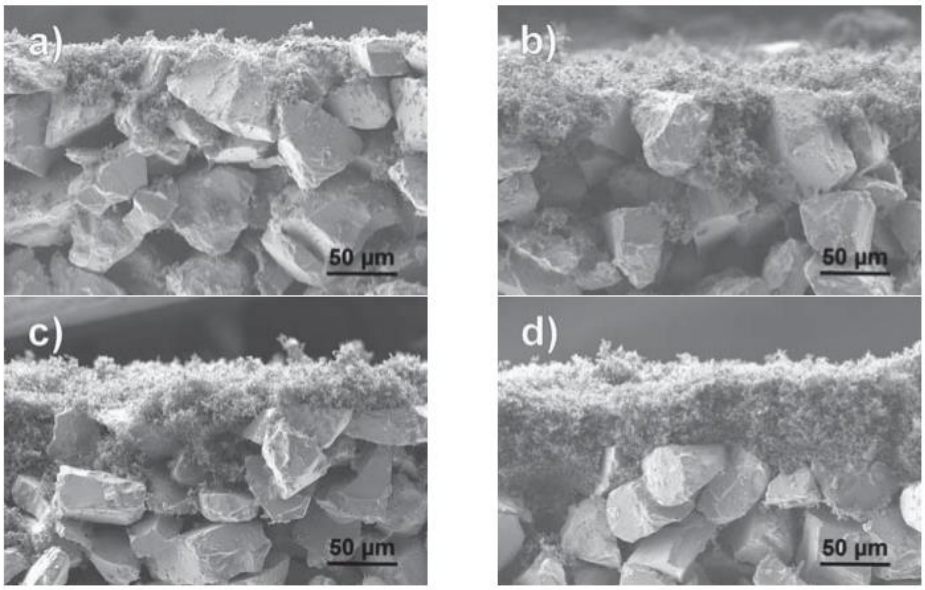

Figure 6: Stages of a DPF substrate loaded with PM to illustrate the formation of the soot cake. Adapted from [24].

Previous work in our group has shown that DPFs are inadequate for GDI particulate capture because the particles are smaller and there are fewer of them in GDI exhaust, as shown in **Figure 3** [27, 28]. Due to the smaller size and lower concentration in comparison to diesel, GDI particulate will not lead to the formation of a soot cake in the filter. In addition, due to higher GDI exhaust temperatures, the concentration of particulates will be further reduced by oxidation, making cake formation even less likely [29]. Therefore, there is need for a gasoline-specific particulate filter (GPF) to reduce PM emissions for GDI vehicles [11, 30].

To achieve the required filtration efficiency, it is logical to use filters with smaller pores sizes. The smaller pores would likely be able to capture the smaller PM. However, smaller pore sizes are associated with a higher pressure drop across the filter, also known as the backpressure penalty with respect to engine operation [24]. Backpressure on the engine decreases fuel

efficiency and increases CO_2 emissions [11], as it decreases the amount of intake air available for combustion and disrupts combustion. GDI engines are known to be more sensitive than diesel engines with respect to backpressure; thus, minimizing the pressure drop across the GPF is vital [31]. Therefore, simply creating filters with smaller pores is not a valid solution, because it does not co-optimize filtration efficiency and pressure drop.

The GPF and DPF are very similar, so many of the strategies developed for particulate filters intended for diesel applications should also be useful to improve GPFs [8, 24]. Konstandopolous and Johnson first noted the fuel penalty caused by DPFs in diesel engines and sought to minimize the pressure drop across the ceramic monoliths in 1989, prior to legislation requiring their use. Variations in geometry, porosity, size, material of construction, channel density, and other methods have been investigated as ways to reduce pressure drop across particulate filters and improve capture efficiency [21, 25, 28, 32]. Notably, Hashimoto *et al.* found that increasing porosity in DPFs decreases the pressure drop across the filter [33]. Boehman and colleagues found that applying coatings of granular silicon carbide to particulate filters can increase the filtration efficiency by replicating a soot cake [34]. While the coated filters had an increased backpressure, they allowed for the use of courser substrates with thinner walls, which can decrease backpressure [34-36]. Therefore, it is reasonable to believe that the combination of a coating to increase the filtration efficiency and using thin, highly porous walled GPFs has potential as a method for co-optimizing filtration efficiency and backpressure, which is the motivation for this work.

The coating material of interest in this work simulates the ash byproduct produced in ICE combustion because it is inexpensive, readily available, and readily collects on the walls of a DPF

or GPF [37]. Ash is the name for the inorganic materials such as metals from lube oils or engine wear that collect in a filter and are not removed by regeneration. Ash can form a plug and increase the pressure drop across filters, which reduces the fuel economy of a vehicle and the time between filter regenerations [38, 39]. A pseudo-cake ash layer on the filter walls is likely to improve filtration efficiency like a soot cake layer. This can create a use for the ash, which is otherwise considered a waste byproduct. Though an increase in backpressure from excessive ash buildup in a filter has been observed [37-39], a pseudo-cake layer could be much thinner than the end-of life buildup seen in heavy-duty diesel DPFS and therefore may not lead to similar unacceptable pressures. Ford recently presented work indicating that a thin layer of ash, deposited to form a pseudo-cake, had significant improvement in filtration efficiency, but further investigation of the effect on backpressure is required [40]. The grain size of the cake layer particles used will also have an impact on both criteria. There is a need to determine an optimal size that will preferentially block larger pores where particle slip is likely, and not block the smaller pores or penetrate the substrate walls, occluding gas flow.

This study uses uncoated GPFs of different wall thicknesses and cell densities to determine which of the three sample types has the lowest filtration efficiency and lowest pressure drop. I hypothesize that using ash-like particles similar in size to, or larger than, the mean pore diameter will allow us to maintain the highest possible porosity for the substrate as the ash layer performs cake filtration on the surface without a significant increase in pressure drop across the filter. Though PM from GDI engines consists of carbonaceous soot of a generally spherical nature with a distribution shown in [41], for this work, ammonium sulfate particulates were used due to lack of access to a GDI engine. The near spherical shape of the salt particles,

availability of the salt, and ease of regeneration by water rinsing were the reasons for this choice in this study and previous work in our group [28], where we have demonstrated the ability to create a particle distribution with a peak between 80 and 90 nm, like soot formed by GDI engines [17].

CHAPTER II

EXPERIMENTAL SETUP

2.1 Gasoline Particulate Filter Samples

Three commercially available Silicon Carbide filter samples sold as GPFs (Dinex, Denmark) were investigated in this work. The 300-08 GPF samples were not initially used for baseline study, but they were implemented for the pseudo-cake modification stage to gather additional data on the impact of the modifications, adding an additional wall thickness and porosity to the permutations studied and they are included in **Table 2** below for that reason. The three primary filters are shown in **Figure 7**, with characteristics for all four samples listed in **Table 2**. All filters are honeycomb wall-flow monolith GPFs with alternately plugged channels, as described earlier and shown in **Figure 5**. Each filter type has three replicates identified by its cell density-measured wall thickness and A, B or C within the same group.

Table 2: GPF sample characteristics.

Filter Sample	Porosity (%)	Plug Length (mm)	Wall Thickness (mm)	Cell Density (cpsi)	Channel depth (mm)
300-08	51-53	5.7	0.254	300	69.7
300-10	56-58	8.4	0.305	300	67
300-12	61-63	8.4	0.405	300	67
200-15	59-63	11.6	0.405	200	63.8

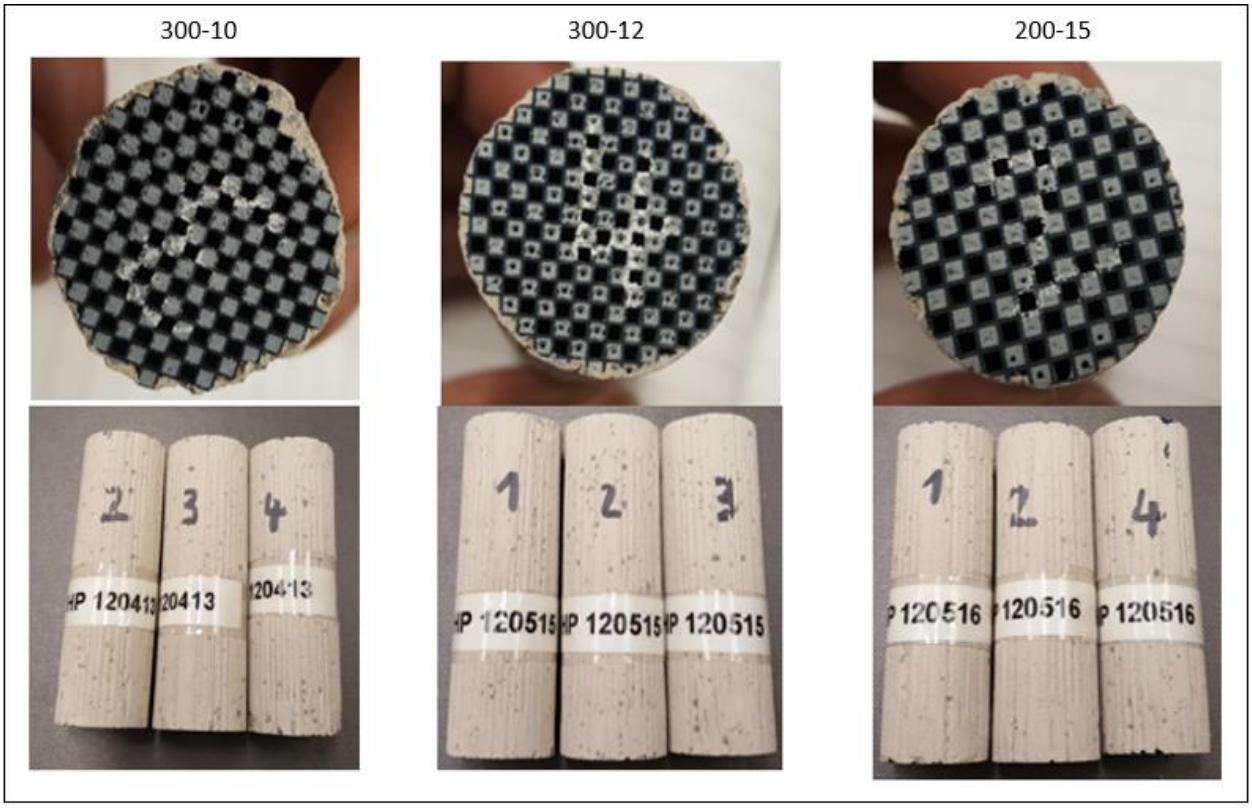

Figure 7: The main three GPF samples used for this study. Each filter type has three replicates identified by cell density, wall thickness and A, B or C within the same group.

2.2 Experimental Setup for Measuring Filtration Efficiency and Backpressure

A SolidWorks model of the experimental setup is shown in **Figure 8**. Building air was HEPA filtered before it enters the system (1), where it flowed to the atomizers (2) and mass flow controller (MFC, 4). Particulates were generated by atomizing an ammonium sulfate solution in one or both TSI Model 3076 Constant Output Atomizers (TSI, MN, USA). A 1 M ammonium sulfate solution was aerosolized with a single atomizer for the 15,000 hr^{-1} and 30,000 hr^{-1} space velocities and a 3 M solution when using both atomizers for a 60,000 hr^{-1} space velocity. The particle-laden vapor in air was dried as it flowed through two silica gel gas driers (3) in series. The MFC (4) was used to change the experimental total flow rate to the filter sample by pushing filtered air into

the system where it mixed with the dried particulate-laden airflow coming from the driers. The concentration of particles in the flow was kept constant while investigating the sample filter behavior at different space velocities by using the MFC and one or two atomizers, as shown in **Figure 10**. The particle-laden flow then passed through the filter sample, held in the filter chamber (5). A single Scanning Mobility Particle System (SMPS, TSI, Minneapolis, MN) consisting of an electrostatic classifier (6), Model 3080 differential mobility analyzer (DMA, 7, TSI, Minneapolis, MN) and Model 3787 water-based condensation particle counter (CPC, 8, TSI, Minneapolis, MN) was used to measure the size-dependent particle concentration in the flow both the upstream and downstream of the filter sample. Valves were used to open and close the constant slipstream flow to isolate upstream or downstream samples. The backpressure, or pressure drop across the filter, was measured using a differential pressure transducer (DPT, MKS, Andover, MA). The exiting flow from the system was exhausted to a hood.

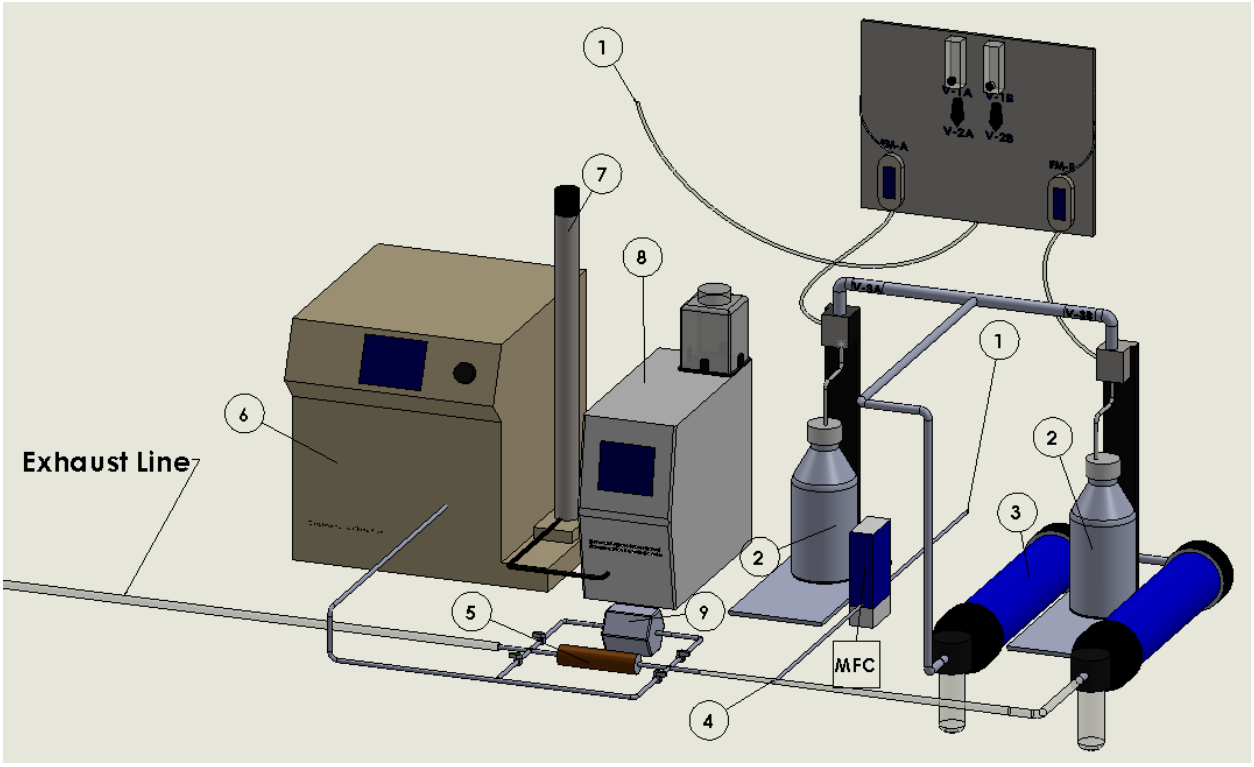

Figure 8: Depiction of experimental set-up. Air is filtered by a HEPA filter and enters the system (1). Filtered building air flows in the atomizers (2) and to the MFC. The particle laden vapor is dried as it flows through the dryers (3). The MFC pushes filtered air into the system to merge with the dried aerosol (4). The mixed air passes through the filter chamber (5). A slip stream is taken through the classifier (6), DMA (7) and CPC (8). The DPT (9) uses ports on either side of the filter chamber to measure pressure drop. The exit flow is sent to the exhaust hood.

The size-dependent particle concentration in the gas was recorded in 30-minute increments for a total of 5 hours, both upstream and downstream of the filter. Five replicate measurements were taken for each position at each time increment, to enable error analysis. For a single experiment with constant space velocity, comparison of the particle counts in each size bin allowed for calculation of filtration efficiency.

Table 3: Volumetric flow rate of particle laden and makeup air for each space velocity

Space Velocity	15,000 hr^{-1}	30,000 hr^{-1}	60,000 hr^{-1}
Total Flow (Lpm)	9.55	19.10	38.21
Atomizer Air (Lpm)	1.60	1.86	3.40
Makeup (Lpm)	7.95	17.24	24.45

The differential pressure transducer simultaneously measured the instantaneous pressure drop at each time point. Valves were used to close off the pressure transducer inlets while not recording pressure in order to avoid salt buildup. Each filter sample was tested in a fresh, never used state, and in post-regenerated state. For the post-regenerated samples, at least 3 replicates of the time-lapse experiment were conducted at each of the 3 space velocities of interest on the filter samples (3 types x 2 samples x 3 replicates of each), as shown in **Table 4**.

Table 4: Data collection matrix for unmodified GPFs. Trials a minimum of 4 days apart for water bath regeneration.

	Sample	15000 hr^{-1}	30000 hr^{-1}	60,000 hr^{-1}
200-15	A	R1, R2, R3	R1, R2, R3	R1, R2, R3
	B	R1, R2, R3	R1, R2, R3	R1, R2, R3
300-10	A	R1, R2, R3	R1, R2, R3	R1, R2, R3
	B	R1, R2, R3	R1, R2, R3	R1, R2, R3
300-12	A	R1, R2, R3	R1, R2, R3	R1, R2, R3
	B	R1, R2, R3	R1, R2, R3	
	C			R1, R2, R3
300-08	F			R1, R2, R3

Between experiments, filters were washed in a bath of heated, distilled and deionized water. The wash water was changed daily for four days. The clean filters were then dried in a vacuum oven.

2.3 Filter Modification

To examine the hypothesis that a pseudo-cake would improve filtration efficiency without a large backpressure effect, two powdered materials were used to load the GPFs: silicon carbide (SiC) and calcium sulfate ($CaSO_4$). The materials were used because of the similarity of $CaSO_4$ to vehicular ash and the previous filtration efficiency improvement to DPFs that both materials exhibited [34]. Furthermore, silicon carbide can be bonded to the filter walls and kept in place by heating, which would make manufacturing simpler. Both pseudo-cake powders had a grain size of approximately 37 μm in diameter (400 mesh). This size was chosen because it is larger than the median pore diameter of each GPF; therefore, it is possible to form a cake on the surface of the walls and only penetrate the larger pores. Smaller grain sizes would likely enter smaller pores and drastically increase pressure drop, which was to be avoided.

To disperse the material and deposit a cake on the filter walls, the MFC, a Swagelok union tee fitting with a cap, and tubing were assembled as shown in **Figure 9**. To account for wall adhesion and other losses in the system, about 130% of the final load was placed into the loading chamber. The cap was secured to the union tee to seal the loading chamber. The MFC was turned on to the maximum flow rate of 40 Lpm to entrain the material and deposit it on the walls of the GPF. The MFC remained on for 5 minutes as the material was deposited into the GPF.

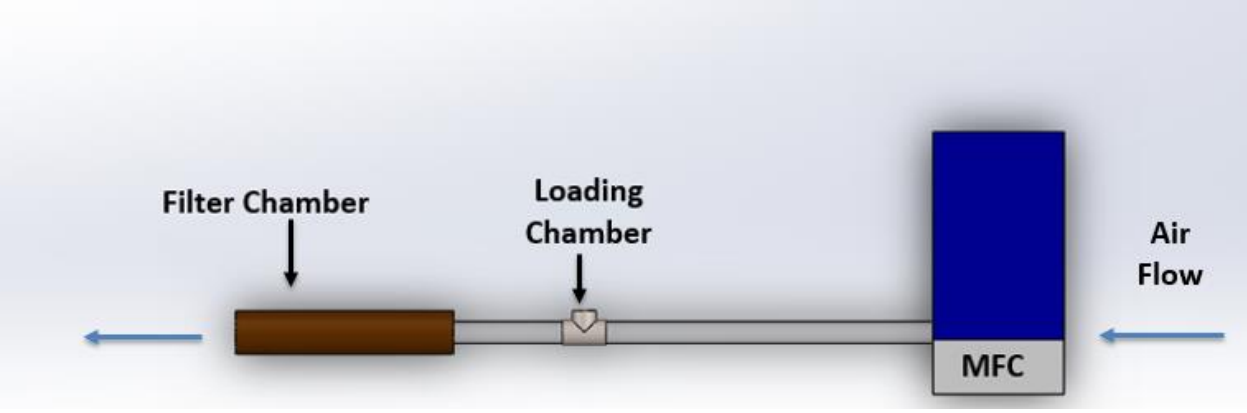

Figure 9: Representation of the setup for loading the GPFs. HEPA filtered air flowing from the MFC at 40 Lpm entrains the material in the loading chamber and propels it into the filter.

The final mass of the filter was compared to the mass prior to loading to calculate the mass of the SiC or $CaSO_4$ retained in the GPF. The density of $CaSO_4$ and SiC are 2.32 g/cm^3 and 3.21 g/cm^3, respectively. The difference in density means the loadings in some instances were identical by mass but not volume of material. The loadings for the GPFs are displayed in **Table 5**.

Table 5: Data collection matrix for pre-loaded GPFs. Loadings not highlighted used only for the initial pressure drop data and not filtration efficiency.

GPF		Initial Mass (g)	Material	Load (g/L)	Final Mass (g)	Loaded Material (g)
200-15	D	28.525	$CaSO_4$	5	28.717	0.192
	D	28.437	$CaSO_4$ & SiC	48	30.3	1.863
	E	27.86	SiC	14	28.39	0.53
	E	27.76	SiC	35	29.11	1.35
	F	27.288	$CaSO_4$	10	27.687	0.399
	F	27.288	$CaSO_4$	15	27.852	0.564
	G	28.868	SiC	20	29.65	0.782
300-10	A	24.48	CaSO4	15	25.045	0.565
	A	24.48	$CaSO_4$	25	25.44	0.96
	B	24.88	SiC	15	25.462	0.582
	C	29.051	$CaSO_4$	10	29.441	0.39
	C	29.051	$CaSO_4$	20	29.824	0.773
300-08	A	21.691	SiC	5	21.88	0.189
	A	22.691	SiC	17	23.34	0.649
	B	21.569	$CaSO_4$	16	22.167	0.598
	B	21.506	$CaSO_4$	39	22.99	1.484
	C	21.666	SiC	20	22.45	0.784
	D	21.372	SiC	10	21.752	0.38

The loaded filters were measured for the pressure drop response at the three space velocities used for the baseline measurements with the DPT. For the loadings highlighted in Table 5, a filtration efficiency experiment was performed as well. Increasing space velocity at a constant particulate concentration results in lower filtration efficiency and increased pressure drop, so the loaded GPFs were investigated for filtration efficiency at 60,000 hr^{-1}. Being the highest of the three flow rates, improvement at that space velocity would indicate the minimum filtration efficiency and highest pressure drop that would result from loading.

CHAPTER III

RESULTS AND DISCUSSION

3.1 GDI-like Particle Size Distributions

The ability of the experimental setup to produce particles in the GDI range of 80 to 90 nm is shown in **Figure 10** and **Figure 11**. Specifically, a 1M solution of ammonium sulfate gives a peak particle size of 88.2 nm, which is comparable to PM produced by GDI engines [42]. It was validated that using either of the two atomizers gives an identical distribution with any amount of make-up air from the mass flow controller. For statistical purposes, there was a minimum of 100,000 particles over the size range of interest, 50 to 150 nm, for analysis of the filters. Only one atomizer is necessary to produce the number of particles needed for space velocities of 30000 hr^{-1} and below. Sample calculations of the make-up air and the flow from the atomizer shown in **Equation 1** and **Equation 2**.

$$V = \frac{\pi L D^2}{4} = \frac{\pi}{4}(7.54\ cm) * (2.54\ cm)^2 = 38.2\ cm^3 = .382\ L \quad (1)$$

$$\frac{SV*V}{60} = \dot{V} = \frac{30000\ hr^{-1}*.382\ L}{60} = 19.10\ Lpm \quad (2)$$

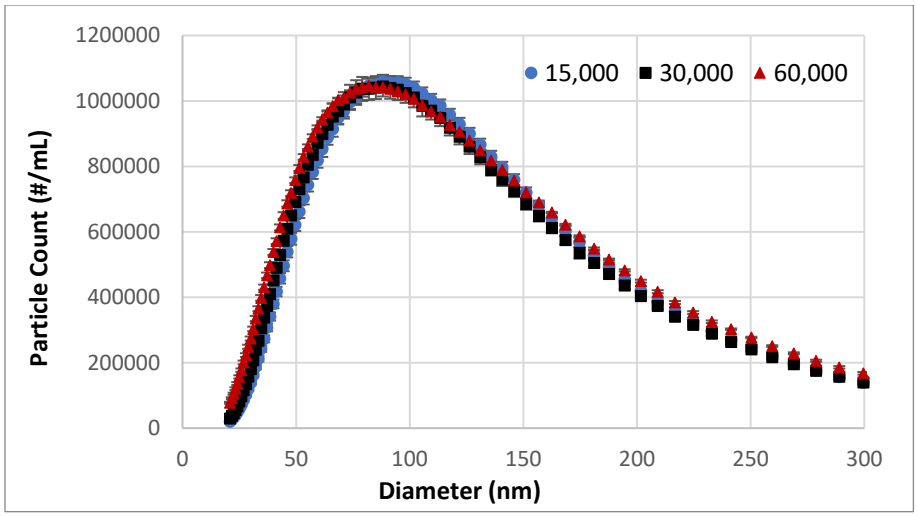

Figure 10: The concentration was kept constant for the air entering the filter chamber at all space velocities. A single atomizer was used for 15,000 and 30,000 hr^{-1} and both atomizers were used for 60,000 hr^{-1}; however, there is no difference in shape of the distribution nor the magnitude of the concentration.

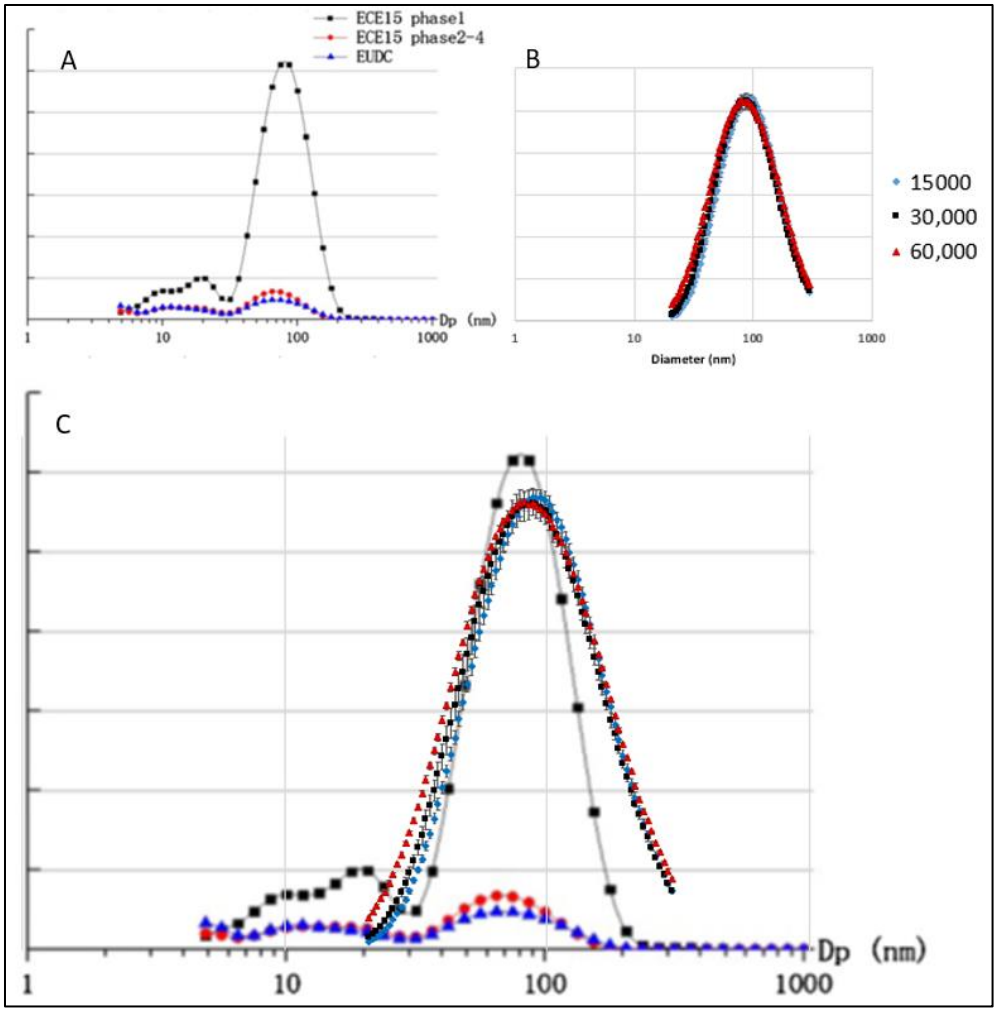

Figure 11: The distribution of PM from a GDI engine at 3 different operating conditions (A) has the same peak and similar distribution to the salt particles (B). The overlay of the salt particles to the PM plot (C) shows the almost identical distributions for the condition with highest concentration of PM. Adapted from [18].

As described previously, upstream and downstream particle concentrations are recorded every 30 minutes until the filter is operating at 99% efficiency. The instantaneous filtration efficiency is calculated using **Equation 3**:

$$\text{filtration efficiency} = \frac{N_b - N_a}{N_b} \quad (3)$$

Where N_b is upstream particle concentration before the filter, and N_a is the downstream or exit concentration after the filter. As the equation indicates, a count of 0 for N_a would give a 100% filtration efficiency. Since there is no regeneration possible with salt particles, and we are loading high concentrations, over the course of the experiment, a particulate cake accumulates on the walls and increases the filtration efficiency, as shown in **Figure 12**.

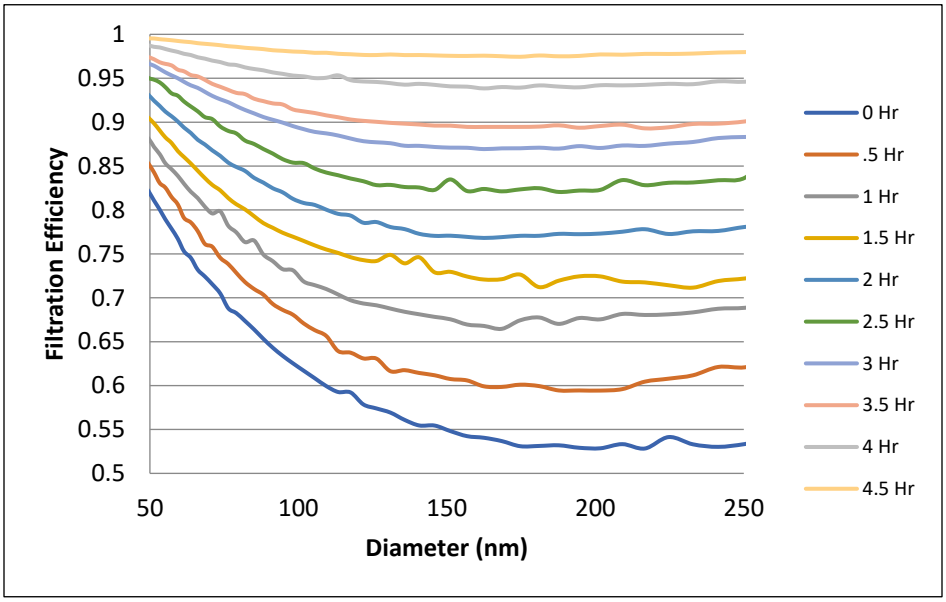

Figure 12: Filtration efficiency over time for 300-10 B at 30,000 hr^{-1}. After 4.5 hours, filtration is 99% efficient, likely due to the formation of a salt particle cake in the filter, which dominates the filtration mechanics.

The increase in filtration efficiency with time, seen in **Figure 12**, is consistent with the known performance of diesel particle filters, where the soot cake that forms during use increases the trapping efficiency of entering particles. Unlike the PM in a GPF, the salt is unreactive in the operating conditions of the investigation; therefore, a cake forms on the filter walls.

3.2 Baseline Performance of Unmodified Filters

Each of the three filter types (200-15, 300-10, and 300-12) was evaluated at three space velocities: 15,000 hr^{-1}, 30,000 hr^{-1}, and 60,000 hr^{-1}. A minimum of 6 replicate experiments were performed on each sample filter type (*i.e.* 200-15 A and 200-15 B at 3 space velocities = 6 replicates on 200-15) to calculate an average size-dependent filtration efficiency and measure the pressure drop as a function of loading across the filter.

3.2.1 Filtration Efficiency and Pressure Drop as a Function of Time

The nine figures below show how the performance, meaning filtration efficiency and pressure drop, of each of the filter types changed as a function of time when keeping filter type and space velocity as independent variables.

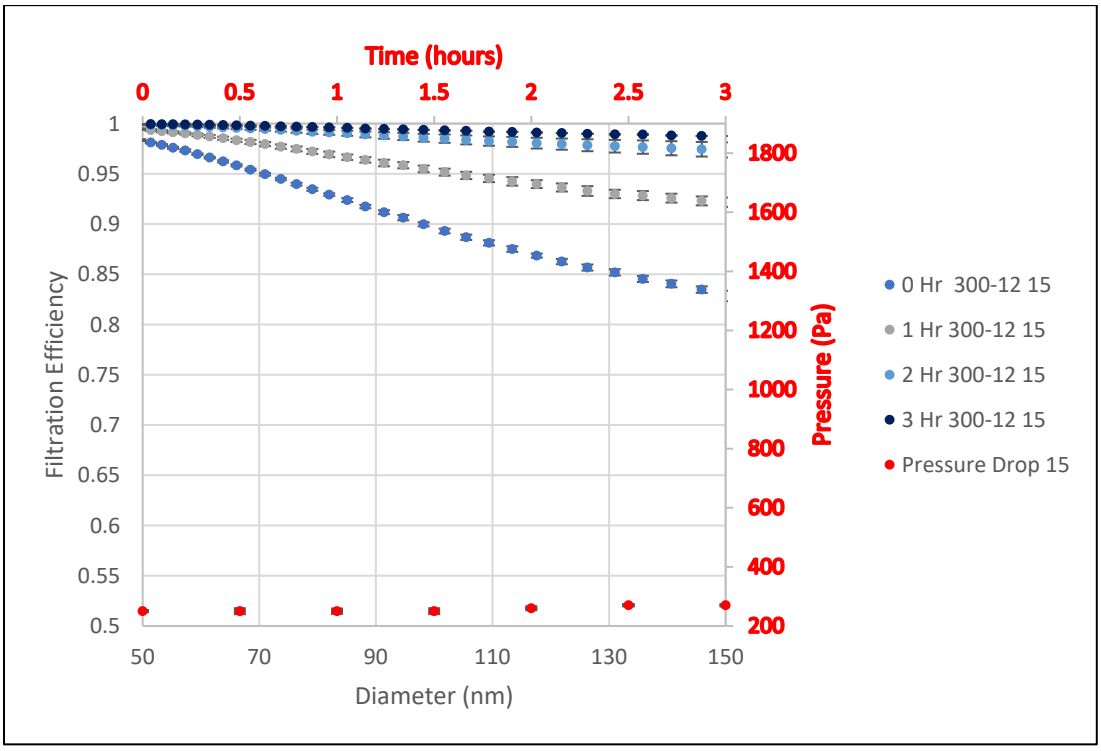

Figure 13: Filtration efficiency and pressure drop for sample 300-12 at 15,000 hr^{-1}.

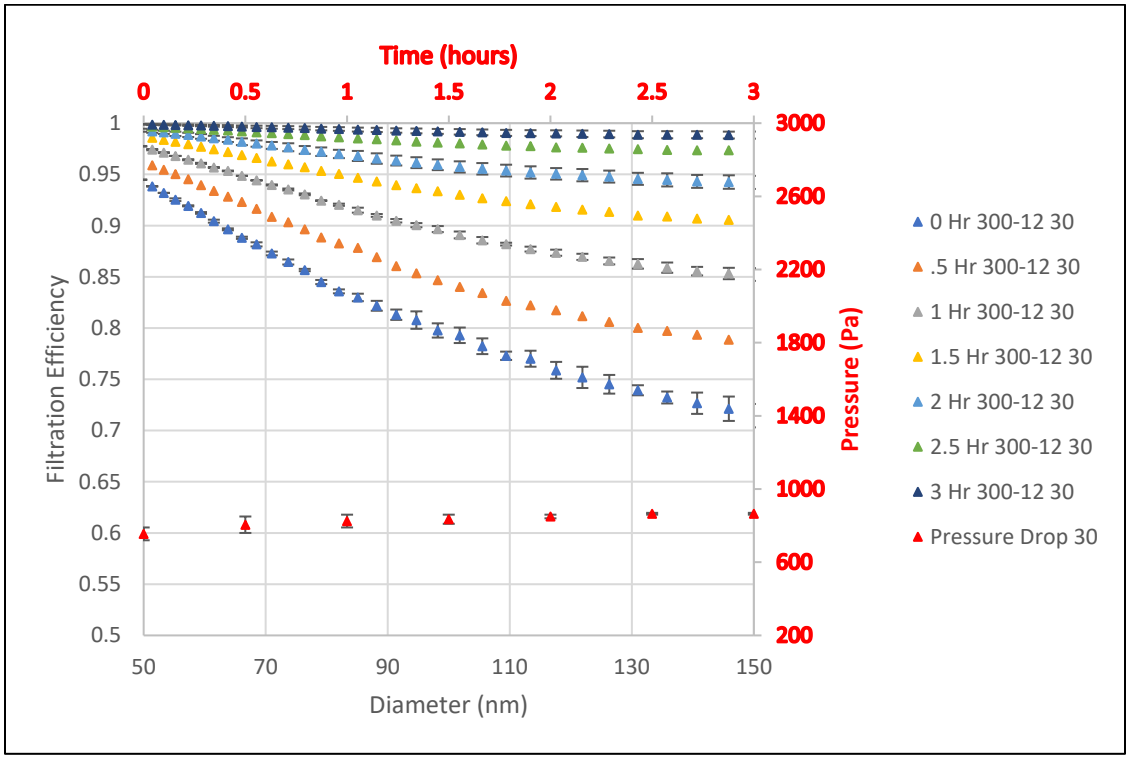

Figure 14: Filtration efficiency and pressure drop for sample 300-12 at 30,000 hr^{-1}.

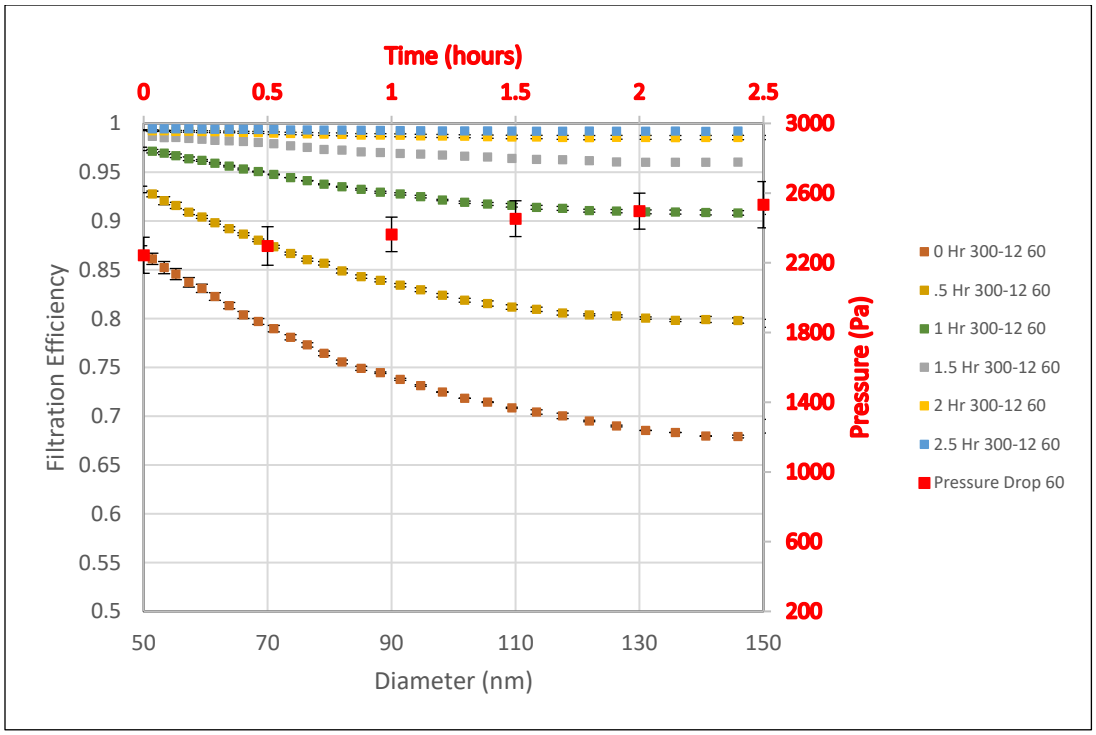

Figure 15: Filtration efficiency and pressure drop for sample 300-12 at 60,000 hr^{-1}.

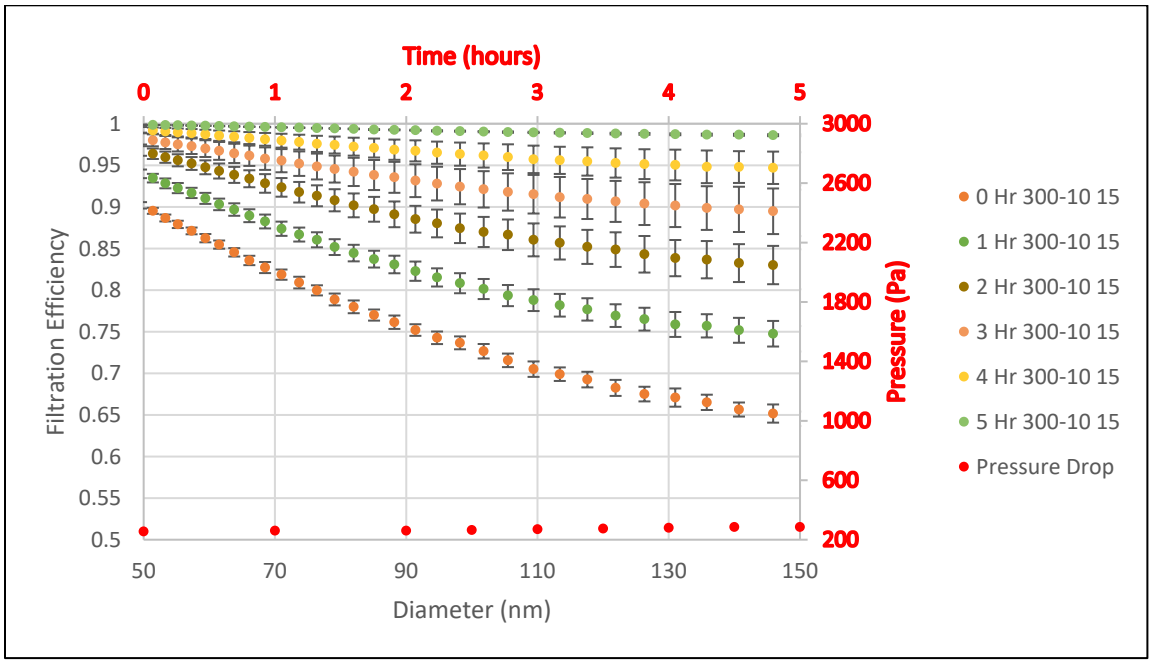

Figure 16: Filtration efficiency and pressure drop for sample 300-10 at 15,000 hr^{-1}.

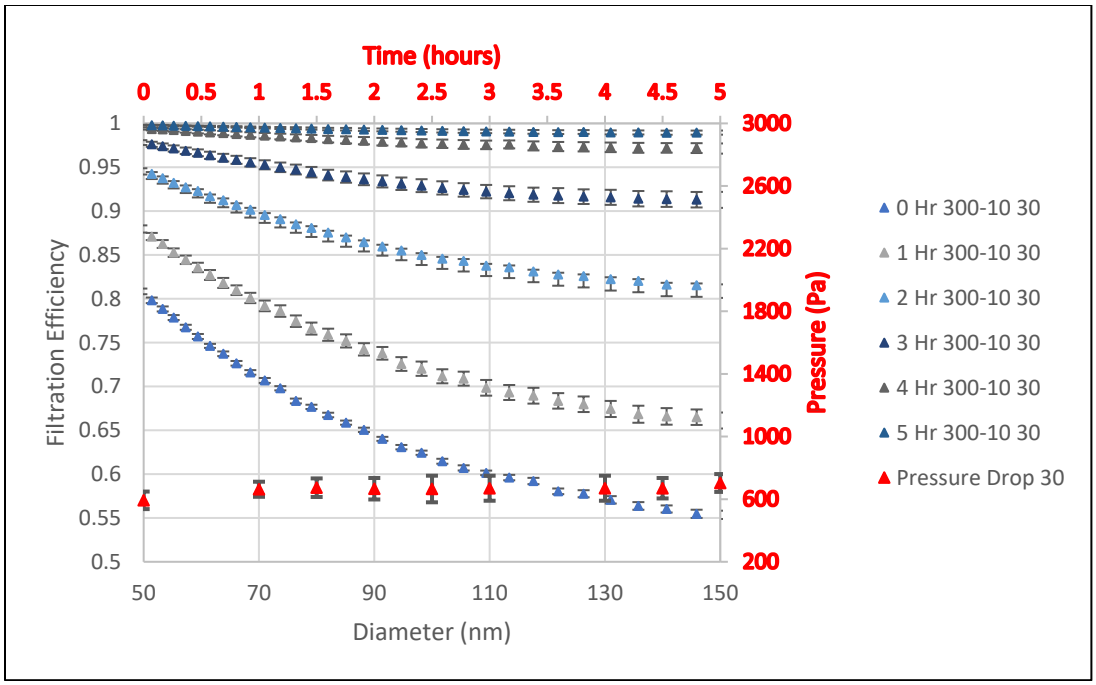

Figure 17: Filtration efficiency and pressure drop for sample 300-10 at 30,000 hr^{-1}.

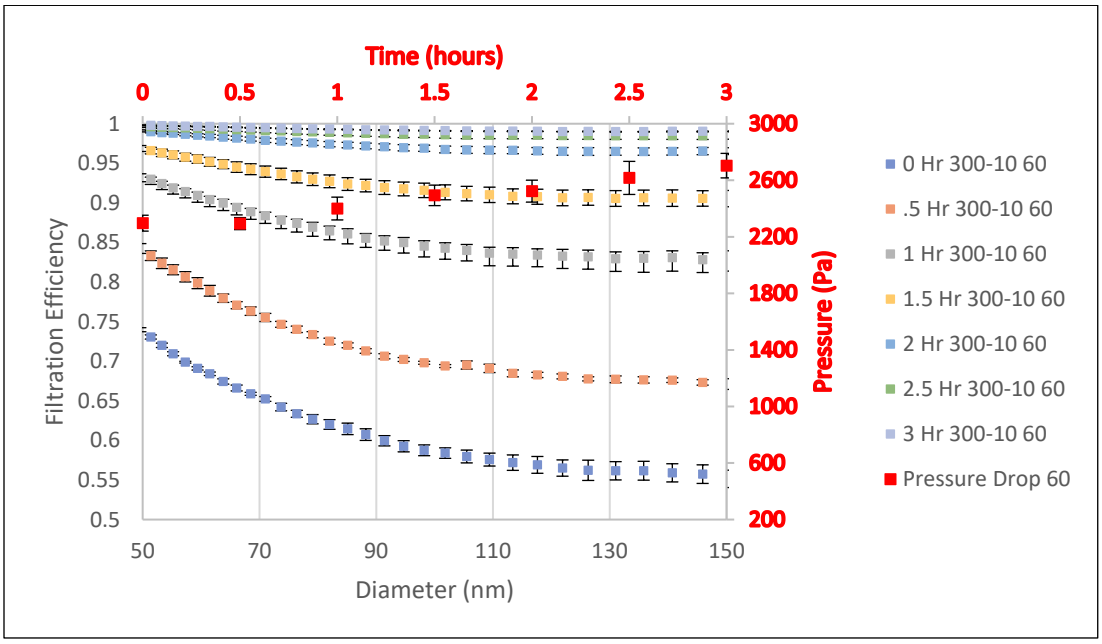

Figure 18: Filtration efficiency and pressure drop for sample 300-10 at 60,000 hr^{-1}.

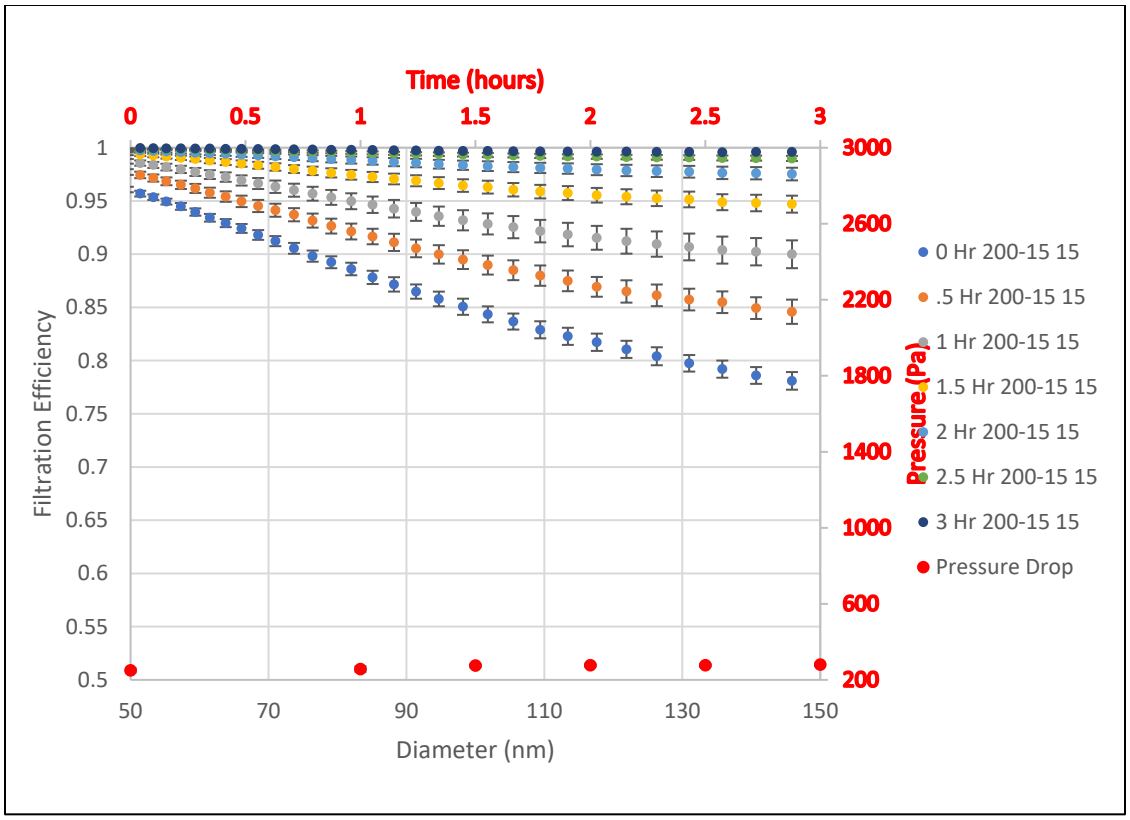

Figure 19: Filtration efficiency and pressure drop for sample 200-15 at 15,000 hr^{-1}.

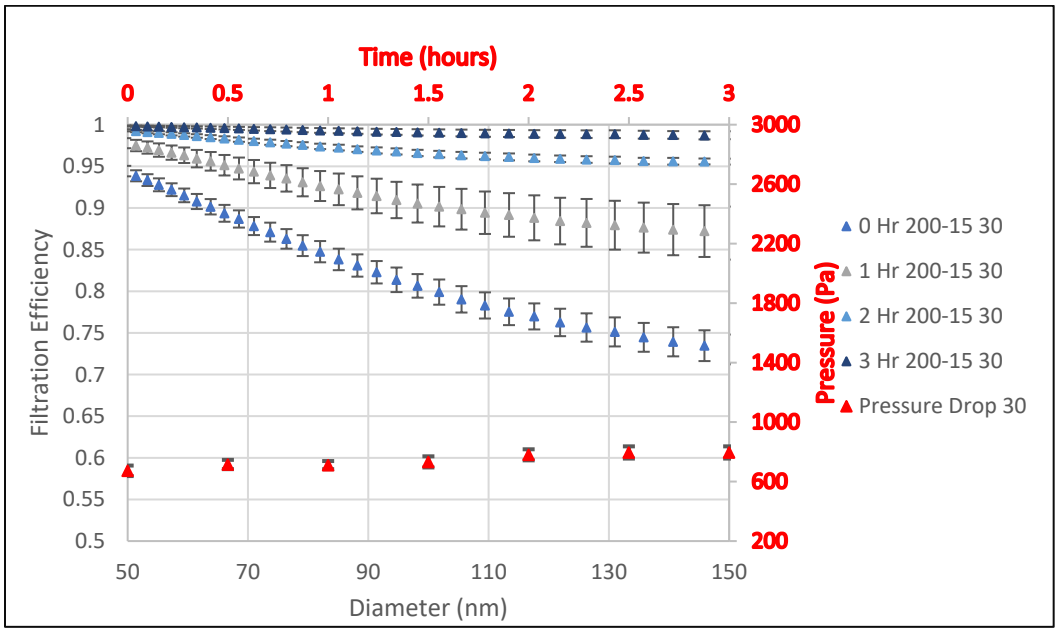

Figure 20: Filtration efficiency and pressure drop for sample 200-15 at 30,000 hr^{-1}.

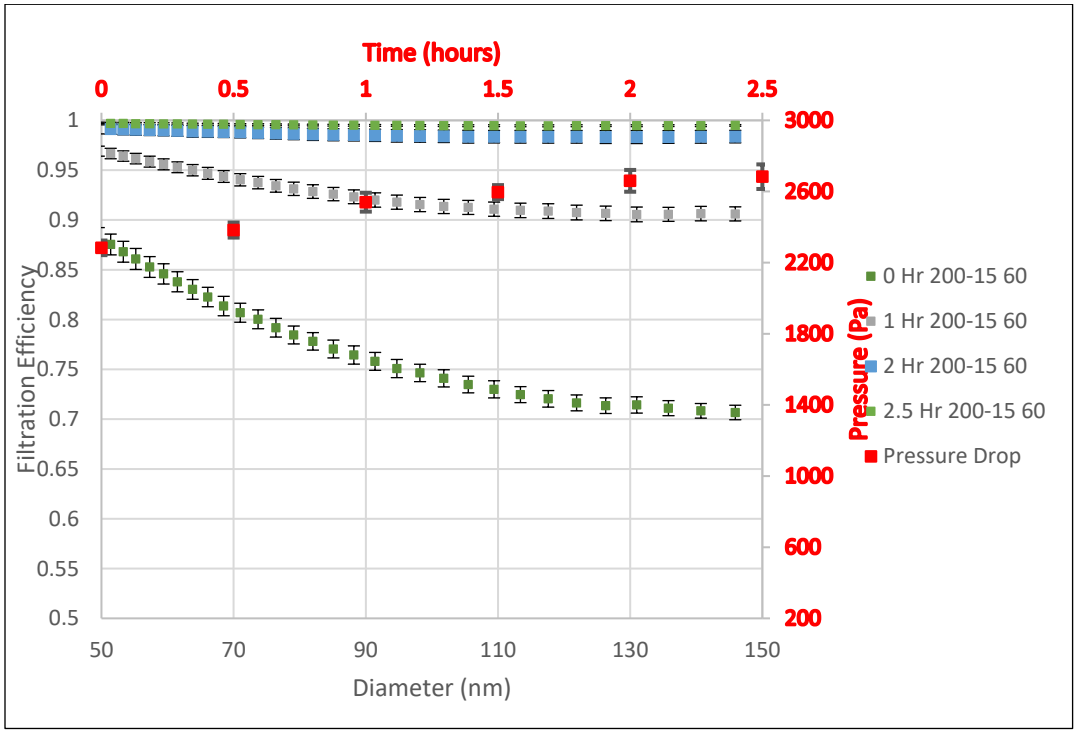

Figure 21: Filtration efficiency and pressure drop for sample 200-15 at 60,000 hr^{-1}.

In each of the figures above, similar trends are observed: filtration efficiency increases with time and salt loading; and, as more salt is trapped in the filter, an increase in pressure drop across the filter occurs. At the lower flow rates of 15,000 hr^{-1} and 30,000 hr^{-1}, the change in pressure drop is much smaller over the entirety of experiment than the initial pressure drop for the 60,000 hr^{-1} experiments. At least two replicates were done on each filter type. The small magnitude of error indicates that samples within the same type behave nearly identically within a given experimental condition.

3.2.2 Filtration Efficiency and Pressure Drop as a Function of Space Velocity

Comparing the results for a single filter type at the three experimental conditions allows the isolation of the impact of flowrate (or space velocity) on the filtration efficiency and backpressure. The following three figures show the filtration efficiency and pressure drop for a single filter at each of the three experimental conditions.

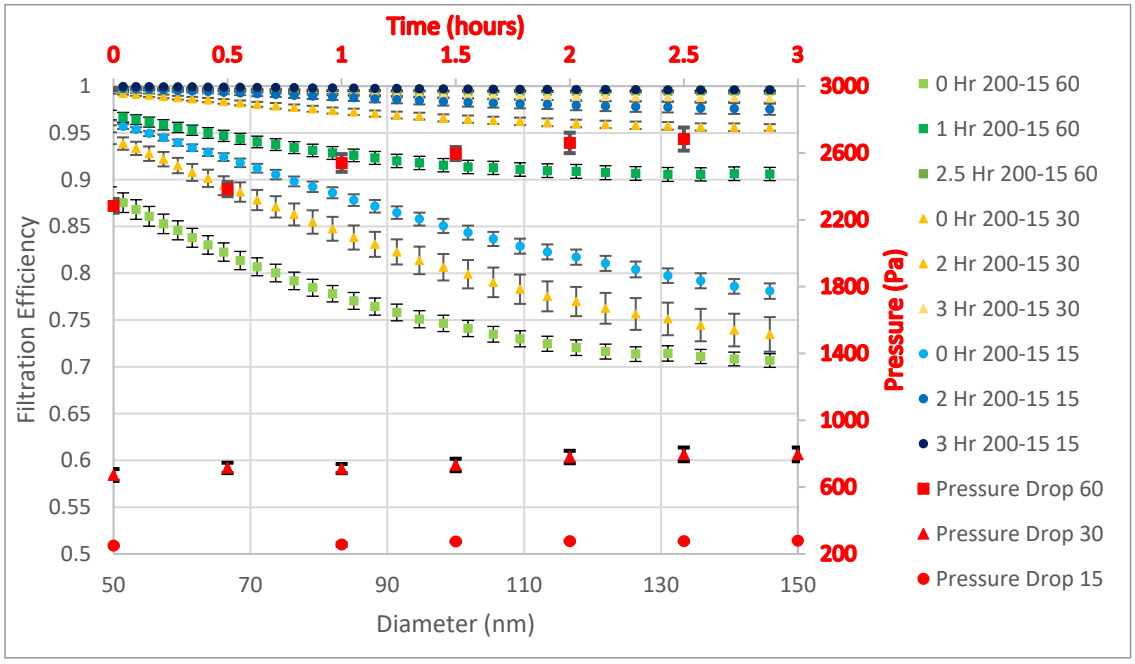

Figure 22: Filtration efficiency and pressure drop of sample 200-15 at each space velocity (15,000 hr^{-1}, 30,000 hr^{-1} and 60,000 hr^{-1}).

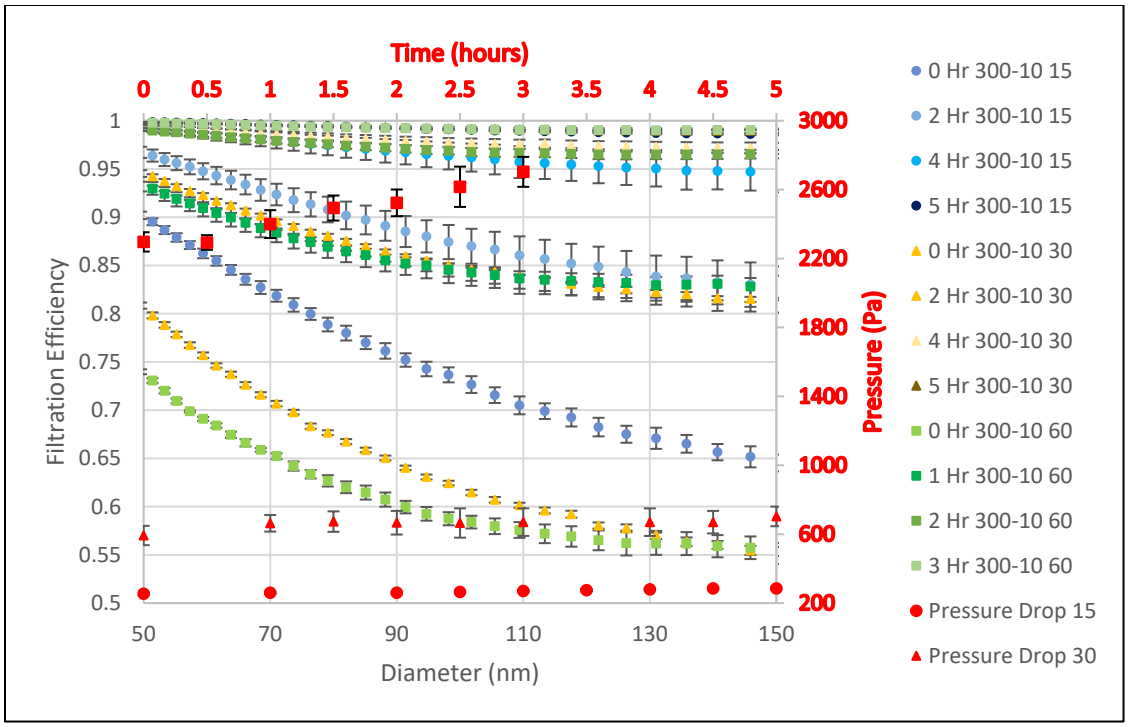

Figure 23: Filtration efficiency and pressure drop of sample 300-10 at each space velocity (15,000 hr^{-1}, 30,000 hr^{-1} and 60,000 hr^{-1}).

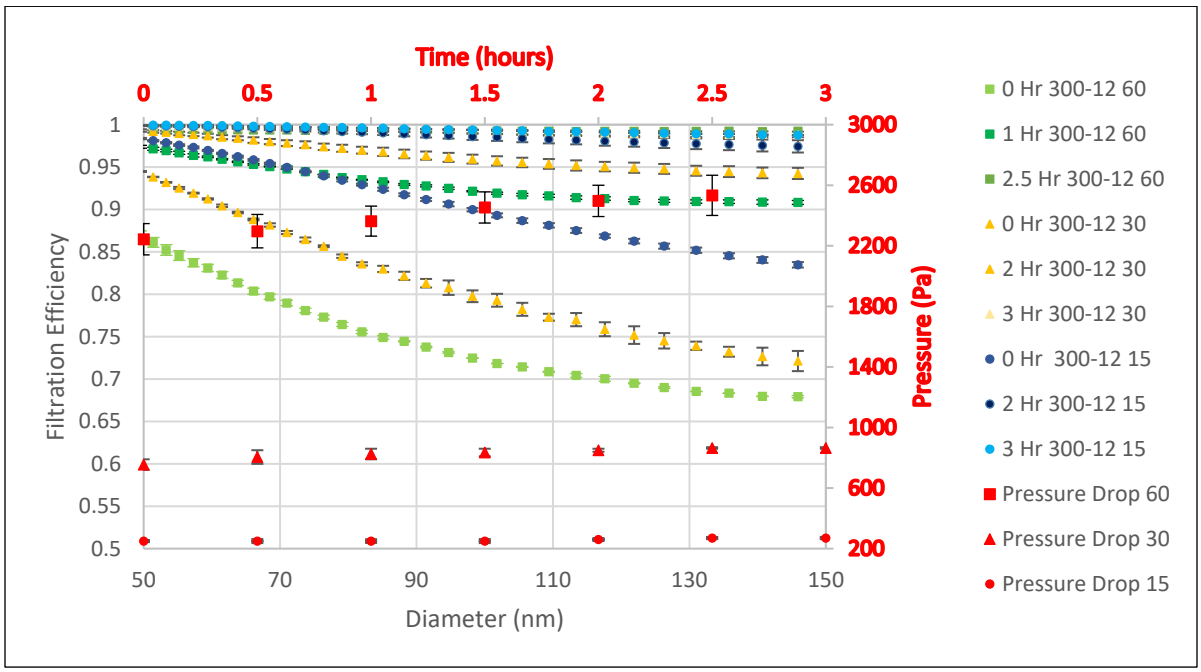

Figure 24: Filtration efficiency and pressure drop of sample 300-12 at each space velocity (15,000 hr^{-1}, 30,000 hr^{-1} and 60,000 hr^{-1}).

Again, there are clear trends, independent of filter type. The lowest initial filtration efficiency is for the 60,000 hr^{-1} and the highest is for 15,000 hr^{-1}, for each filter type. To maintain the same concentration of particles at higher space velocities, significantly more particles are entrained in the air flowing into the filter. With significantly more particle loading per unit time at 60,000 hr^{-1}, a cake forms faster and the GPF reaches 99% filtration efficiency sooner. At low space velocities, the pressure drop across the filter increases very little over time despite the particulate loading forming a cake layer. At higher space velocities, the increased volumetric flow rate results in higher wall velocities and an increased pressure drop across the filter. The formation of a cake layer exacerbates the effects seen with higher space velocity and results in the larger increase in pressure drop over time.

3.2.3 Filtration Efficiency and Pressure Drop as a Function of Filter Type

Comparing the filtration efficiency and pressure drop of the three filter samples at a single flow provides insight to the substrate-specific effects, as shown in **Figure 25** - **Figure 27**.

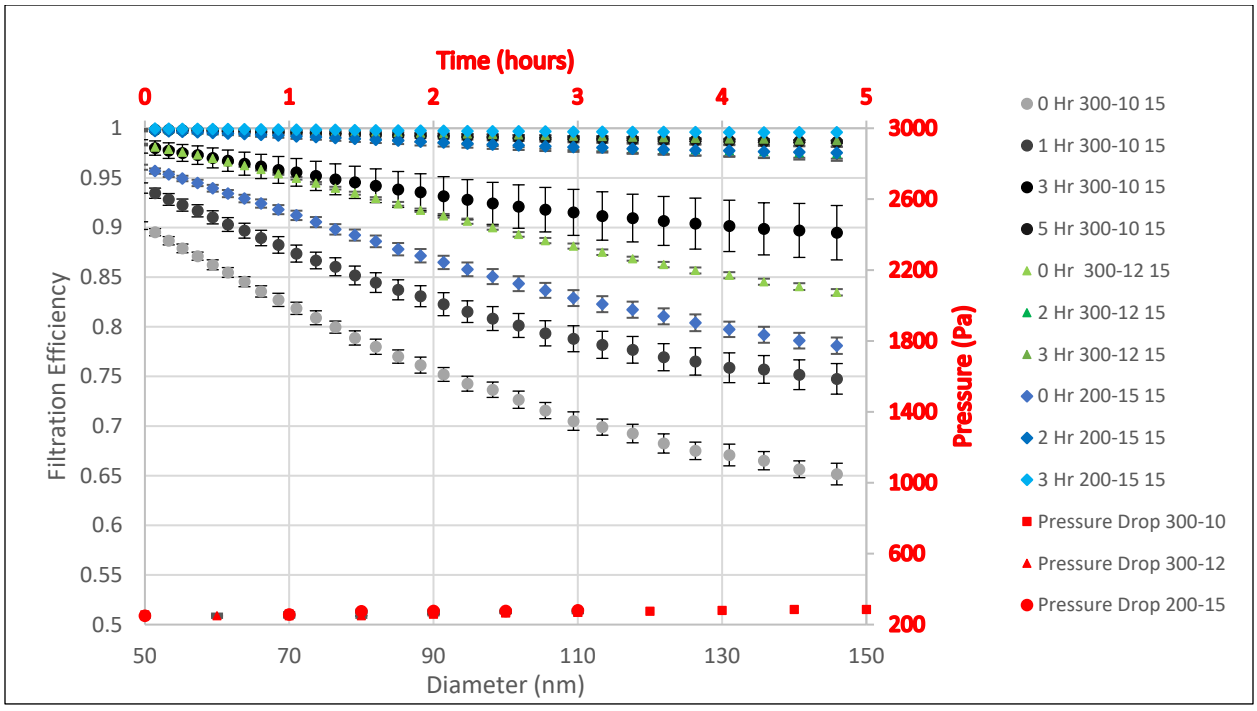

Figure 25: Comparison of filtration efficiency and pressure drop at 15,000 hr^{-1}.

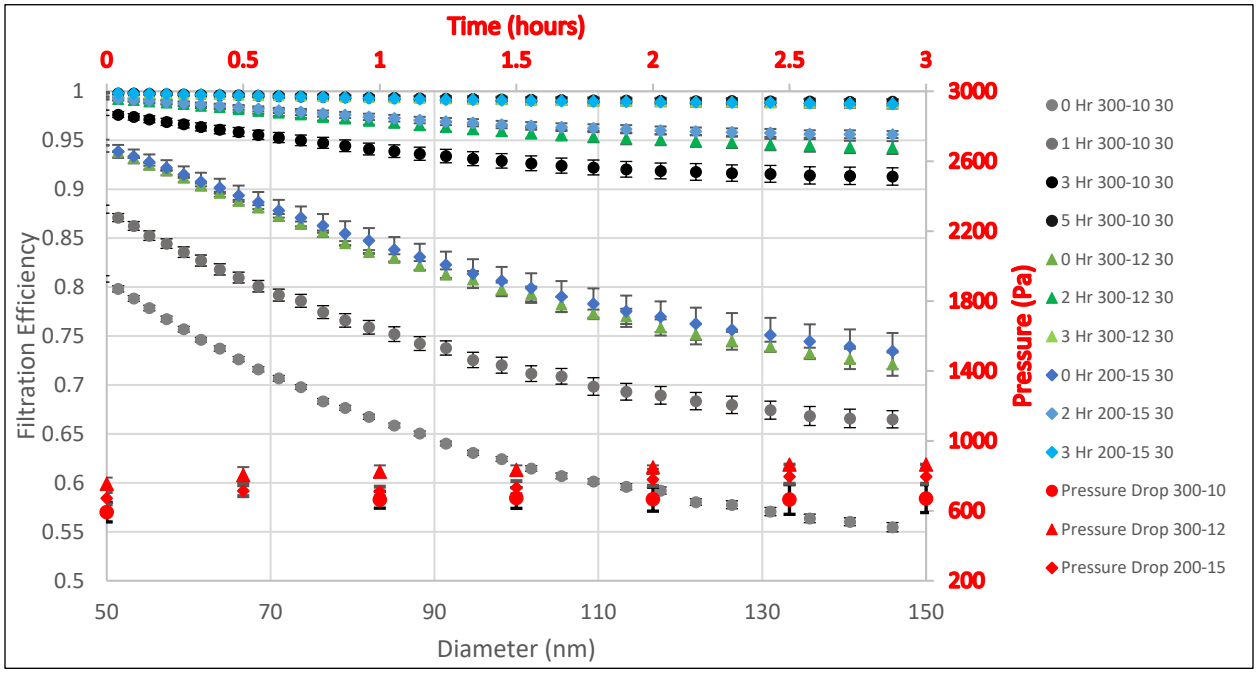

Figure 26: Comparison of filtration efficiency and pressure drop at 30,000 hr^{-1}.

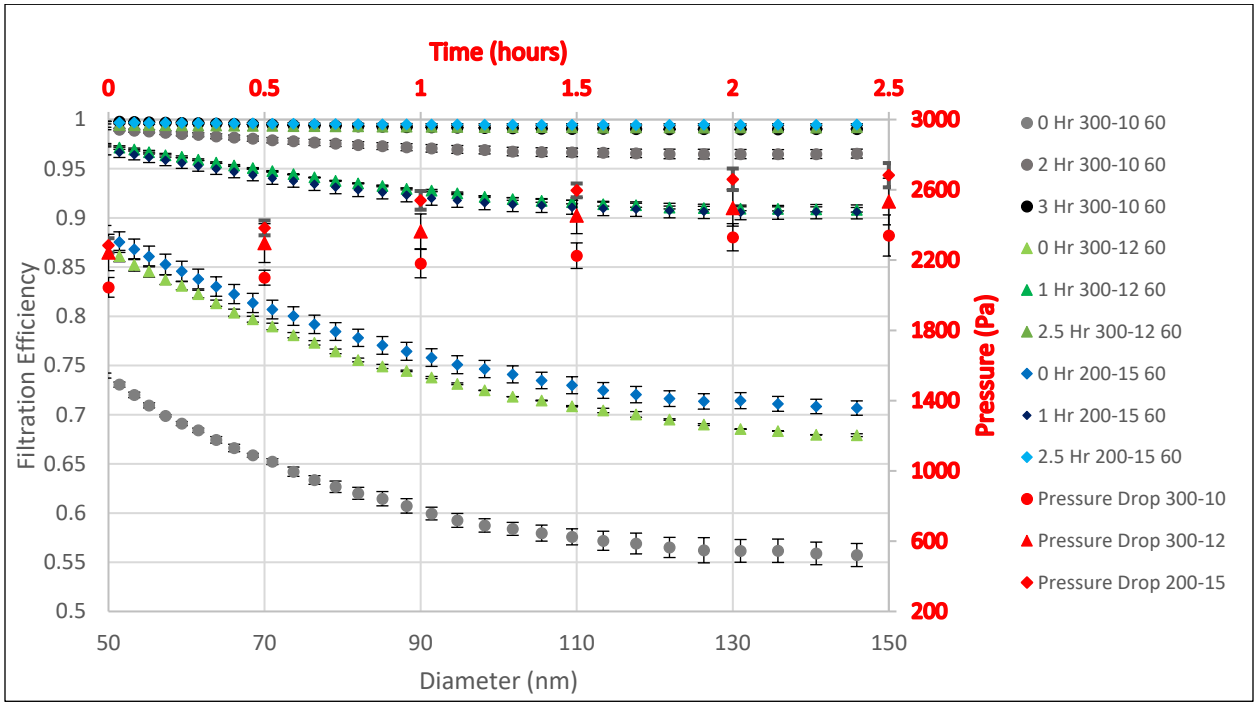

Figure 27: Comparison of filtration efficiency and pressure drop at 60,000 hr^{-1}.

The pressure drop at 15,000 hr^{-1} was measured to be 265±15 Pa, independent of filter type and salt particulate load. At 60,000 hr^{-1}, the difference in pressure drop across the filters has more separation in magnitude as the particulate cake forms over time. Throughout the experiments, 200-15 has the highest pressure drop. It was measured to be 2280 Pa initially and to be 2700 Pa once 99% filtration efficiency was reached. The initial pressure drop of 300-12 is slightly lower at 2240 Pa and 2530 Pa after 99% filtration efficiency. The lowest pressure drop was measured across 300-10, which was initially 2045 Pa and ended at 2350 Pa. For each space velocity, the order of filtration efficiency and pressure drop across the filter from lowest to highest is 300-10, 300-12 and 200-15. Increasing wall thickness and decreasing cell density

coincides with better filtration but higher pressure drop. The sacrifice of filtration efficiency for lower backpressure, the problem to be overcome, is presented here.

The lowest filtration efficiency and pressure drop is seen in filter 300-10, which is the reason it was chosen for modification. For the three space velocities investigated, filtration efficiency is the lowest and pressure drop is the highest at 60,000 hr^{-1}. The response for this space velocity indicates the largest increase to pressure drop the GPF would experience and the minimum improvement to filtration efficiency; therefore, the modification space velocity study was performed at 60,000 hr^{-1}.

3.3 Loaded Filters

The changes in pressure drop and filtration efficiency were measured for the modified GPFs of groups 300-10, 300-08 and 200-15. A baseline for 300-08 was recorded only at 60,000 hr^{-1} to replace the damaged 300-12, which allowed more analysis of the responses. Because of the low pressure drop and filtration efficiency in comparison to 300-12 and 200-15, 300-10 was the focus for improvement. The 300-10 group was last to be modified after seeing the response in 300-08 and 200-15 when they were loaded. The pressure drop for each filter was measured with HEPA filtered air before any particulate was introduced. This allowed measurement at each space velocity while the GPFs remained in an unused condition. Changes in filtration efficiency are most heavily inspected and quantified for particulate near 90 nm in diameter because GDI engines from Ford emit PM with distribution peaks at approximately that size. A simplified loading process was used for the experiment; therefore, some variation to the trends is likely.

3.3.1 Pressure Drop Response for Loaded Filters

Particle-free building air was used at the three space velocities prior to the filtration efficiency experiments. This allowed for load increases and measurement of initial pressure drop to compare to unloaded GPFs without the need of regeneration. **Table 6** shows the pressure drop data for each space velocity for the filters.

Table 6: Pressure drop data for the GPFs both before and after modification. Measurements are rounded to nearest 5 Pascals.

GPF		Unloaded Pressure (Pa)			Loaded Pressure (Pa)				
		15,000 hr^{-1}	30,000 hr^{-1}	60,000 hr^{-1}	Material	Load (g/L)	15,000 hr^{-1}	30,000 hr^{-1}	60,000 hr^{-1}
200-15	D	285	800	2290	$CaSO_4$	5	280	730	2170
	D				SiC	48	410	1000	2490
	E				SiC	14	240	650	1850
	E				SiC	35	290	790	2240
	F				$CaSO_4$	10	290	760	2080
	F				$CaSO_4$	15	290	770	2160
	G				SiC	20	280	720	1890
300-10	A	260	690	1985	$CaSO_4$	25	260	720	2100
	B				SiC	15	260	690	1860
	C				$CaSO_4$	10	260	710	2050
	C				$CaSO_4$	20	280	750	2160
300-08	A	240	670	2020	SiC	5	250	690	2030
	A				SiC	17	260	760	2180
	B				$CaSO_4$	30	300	800	2160
	B				$CaSO_4$	16	270	720	2040
	C				SiC	39	260	720	2140
	C				SiC	20	260	670	1810
	D				SiC	10	250	670	2030

As with the baseline testing, insignificant differences were measured at 15,000 hr^{-1} for most loadings. Increasing the load within a GPF followed the expected trend of increasing the backpressure regardless of filter sample group as more pores were blocked by the facsimile cake. However, the loaded 200-15 pressure measurements were lower than the baseline for almost every load at 30,000 hr^{-1} and 60,000 hr^{-1}, with 48 g/L being the only load measured at a higher backpressure than unloaded. A possibility of damage to the GPFs could explain the decrease in pressure drop from the unloaded to loaded.

At 60,000 hr^{-1}, similar behavior occurred for 300-08 and 300-10 with respect to the unloaded. Loaded with 10 g/L of SiC, 300-08 at was much lower at 1810 Pa than unloaded 2020

Pa, and 300-10B loaded with 15 g/L of SiC was 125 Pa lower than the unloaded. The single deviation from trend within both groups is reason to believe damage to the filter or measurement error could be responsible. Fast flowing material impacting the filter walls could damage a filter, which would decrease any pressure drop across the GPF.

The increases from the lowest loadings to the highest were in the range of 50-100 Pa for every additional 5 g/L of cake material. Less porosity due to obstructed pores causing higher backpressure is consistent with previous findings. The largest loading of 25 g/L for 300-10 resulted in a pressure increase of about 6%; however, a loading of 20 g/L increased the pressure drop 8% to 2160 Pa. The larger pressure drop for a lower loading is possibly attributable to a damaged 300-10A or cake deposition discrepancies.

Full analysis of why the pressure drop across some loaded filters decreased from the unloaded filters would require microscopy to inspect the cake deposition on the walls and the integrity of the walls.

3.3.2 Filtration Response for Loaded Filters

The response in filtration efficiency and pressure drop are displayed in **Figure 28** and **Figure 29.** An increase in filtration efficiency occurs with the addition of a cake. For 200-15, a 5 g/L loading does not significantly increase filtration efficiency above the error for an unloaded GPF. When $CaSO_4$ was preloaded at 15 g/L, an improvement of ~5% filtration efficiency was observed. While the pressure drop for 15 g/L of SiC is about equal to 5 g/L of $CaSO_4$ throughout the salt particle loading, filtration efficiency is only slightly more than 5 g/L of $CaSO_4$ and half as much as 15 g/L of $CaSO_4$. The difference in response to the two materials is likely due to a lower volume of the denser SiC at the same loading. Less volume equates to fewer obstructed pores.

Also, the cake distribution is unlikely to be the same within the GPF. A 5% increase at 15 g/L of $CaSO_4$ does not increase the filtration efficiency to the 94% that would meet standards, but it does provide reason to investigate more preloaded cakes with controlled placement.

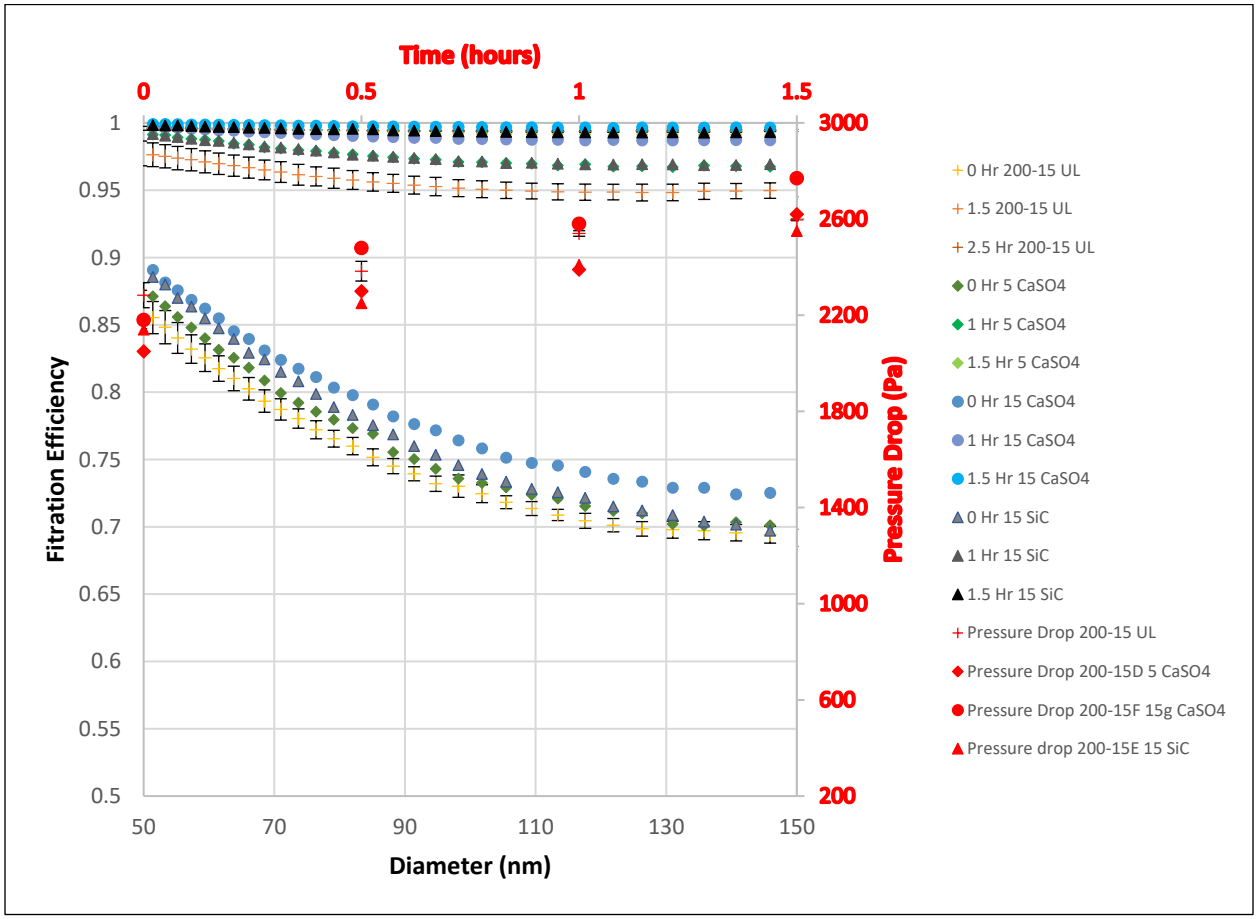

Figure 28: Filtration Efficiency and Pressure Drop of Sample 200-15 Comparison to Loaded

The filtration efficiency experiments on 300-10 show an increase of ~10% in initial filtration efficiency is possible with 20 g/L of $CaSO_4$. The backpressure does increase, unlike 200-15, but at a lower percentage, ~6%, than the filtration efficiency increases. Again, the distribution of the cake on the filter walls was not controlled, so the 25 g/L loading being lower

in both pressure drop and filtration efficiency could be a result of how the cake formed or because of damage to the GPF. However, a 25 g/L load was about 7% more efficient in capturing the salt particles with only a 1% increase to the pressure drop. The increase of filtration efficiency being more significant than the increase to pressure drop gives cause for further investigation of loadings in this range.

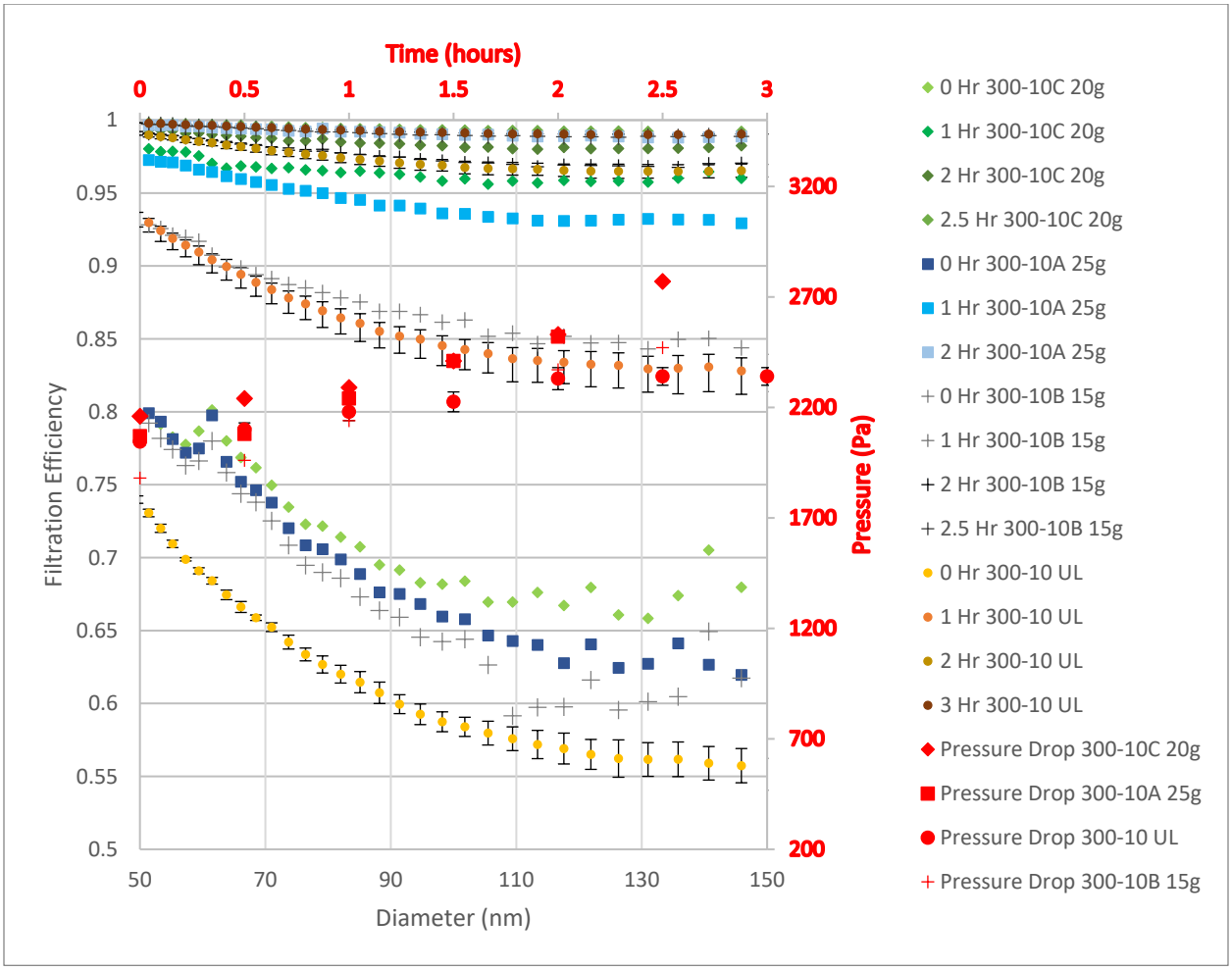

Figure 29: Plots of the filtration efficiency and pressure drop of the loaded 300-10 group for comparison to unloaded.

Both plots show the increase to filtration efficiency that can be achieved using a preloaded cake. Because baseline initial filtration efficiency of 200-15 is much greater than the 300-10, a 10% increase to 300-10 did not achieve the filtration efficiency of the unloaded 200-15, but the pressure drop for 25 g/L was over 200 Pa lower initially. If an improvement of 10% efficiency can be achieved for other filters with higher unloaded filtration efficiency, preloading a cake can be useful in reducing PM emission. While neither plot displays a load that improves a GPF to 94% initial filtration efficiency, the increasing trend with increasing loading is evident within the range of interest, 80-100 nm. Furthermore, no large increases to the pressure were seen. **Figure 30** shows the responses for the modified 300-10 samples.

3.4 Summary

The experiments were proven to be reproducible between regenerations of a single filter sample filter and across filter samples of the same type with respect to time and space velocity. GPFs with the same wall thickness, cell density, and porosity behave very similarly. The small errors on each plot show the pressure drop and filtration efficiency vary only slightly within the filter type groups.

A GPF with thicker walls will remove more particulate, but a higher backpressure will result. Each of the filters showed an inverse relation between initial filtration efficiency and space velocity. These experiments represent the baseline case for each filter type, which will serve as a comparison for the modifications to be investigated.

The pressure drop and filtration efficiency is lowest at 60,000 hr^{-1} and highest at 15,000 hr^{-1}. The modification needs to improve the filtration efficiency of the 300-12 type filter by about 10% at 15,000 hr^{-1} and 25% at 60,000 hr^{-1} to meet the proposed regulation, whereas the 200-15

requires about 10% at 15,000 hr^{-1} and 20% at 60,000 hr^{-1} and the 300-10 filters would require about 20% at 15,000 hr^{-1} and 35% at 60,000 hr^{-1}.

The pressure drop measurement across 200-15 at 48 g/L rising 320 Pa from 5 g/L, a 15% increase, indicates there is no reason to investigate loadings in that range. The filtration efficiency data for 5 g/L having almost no change from the unloaded shows that the loading is too minute. The filtration efficiency plots for 300-10 indicate the possibility of 20-25 g/L, or slightly larger, as a reasonable loading to investigate further. At 60,000 hr^{-1}, which was the space velocity with the lowest filtration efficiency for all filter groups, filtration efficiency increased by about 10% with an initial backpressure increase of 6%, as shown in **Figure 29**.

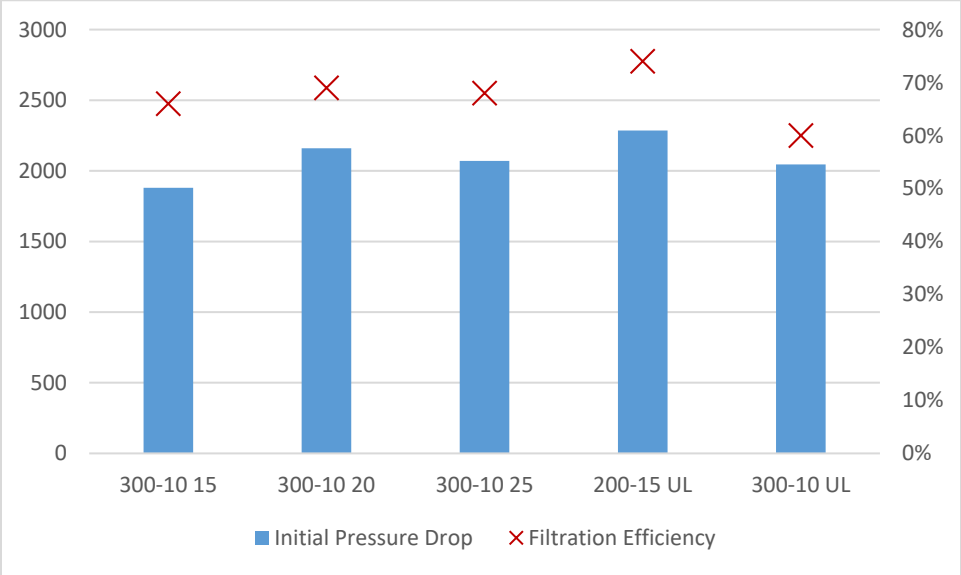

Figure 30: Comparison of modified 300-10 samples to the baseline filtration efficiencies and pressure drops initial condition in the 80-100 nm range for salt particles. UL meaning unloaded and the number indicating the load in g/L.

This modification did not improve the GPF to a filtration efficiency high enough to be compliant with GDI emissions standards. The increase did show the possibility of low pressure increase with a moderate filtration efficiency increase using a preloaded cake. $CaSO_4$, likely due to its lower density, increased the filtration efficiency more than SiC. Furthermore, SiC appeared to damage the GPFs during loading, so an accurate analysis of pressure drop for this material cannot be concluded.

CHAPTER IV

CONCLUSIONS AND FUTURE WORK

A GPF will have a lower filtration efficiency for air at a higher flow rate than air at a lower flow rate and identical concentration; therefore, the filtration efficiency at 60,000 hr^{-1}, or the highest space velocity the engine operates under, should be used to determine the efficiency of the GPF.

The experiments showed that higher porosity and thinner walls correlate to lower pressure drop and filtration efficiency for GPFs. Improving filtration efficiency for the 300-10, which was the thinnest and most porous, by increasing filtration efficiency more than pressure drop indicates a useful modification.

The modifications to the filters were implemented to investigate the possibility of using a preloaded cake to overcome the opposed relationship of backpressure with filtration efficiency. Increased loading of a pseudo- cake onto the filter walls increases the backpressure, but a filtration efficiency improvement of about 10% that increases backpressure by 115 Pa (<6%) is achievable. Neither the $CaSO_4$, nor the SiC loads investigated increased filtration efficiency enough to reduce GDI PM emissions within compliance. However, the increase in filtration efficiency for 300-10 was measured about 6% below the unloaded 200-15, while the pressure drop was about 8% lower. Thus, it is possible that a preloaded cake layer can increase the filtration efficiency at a faster rate than it increases pressure drop. The larger increase of the former would make applying cakes to thinner walled GPFs a more feasible way to improve performance than manufacturing thicker walled counterparts. Combined with other GDI

technology aimed at reducing PM production, it is possible that a GPF can be improved with a pseudo-cake to meet increasingly stringent regulations without greatly increasing backpressure.

The improvement to the GPF using when my method of depositing a cake indicates further investigation is needed. Microscopy on the loaded filters to find out the degree of homogeneity to which the cake deposited can be valuable because there is a possibility of higher filtration efficiency increase with a homogeneous preloaded cake layer. A filtration experiment on a GPF of 300-10 with a pressure drop equal to 200-15 can better clarify whether a cake will improve filtration efficiency more than it increases pressure drop. Investigation into the diameter of the cake particles, which affects the obstruction of pores, needs to be conducted. Changing grain sizes will affect the magnitude of the backpressure and filtration efficiency response. Additional research into the mechanical integrity of GPFs being loaded with a cake is also needed to assure no damage results from loading. Visual damage to GPFs was observed on the exterior, and the reduced pressure drop of the loaded 200-15 samples from the unloaded raises the question of internal damage to the walls. The use of vehicular ash as the cake material and using GDI PM instead of salt can also add value to a future study. Data from the experiments can be compared with models. It can aide in further investigation into cake depositions in the attempt to improve filtration efficiency without a significant backpressure expense.

REFERENCES

1. EPA, *Summary of the Clean Air Act*. 2017: EPA.gov.

2. Baker, J.A., *Particulate Matter Regulation and Implications for the Diesel Engine*. 1998, SAE International.

3. Harrison, R.M. and J. Yin, *Particulate matter in the atmosphere: which particle properties are important for its effects on health?* Science of The Total Environment, 2000. **249**(1): p. 85-101.

4. Anderson, J.O., J.G. Thundiyil, and A. Stolbach, *Clearing the air: a review of the effects of particulate matter air pollution on human health.* Journal Of Medical Toxicology: Official Journal Of The American College Of Medical Toxicology, 2012. **8**(2): p. 166-175.

5. Hoek, G., et al., *Long-term air pollution exposure and cardio- respiratory mortality: a review.* Environmental Health: A Global Access Science Source, 2013. **12**(1): p. 1-15.

6. EPA, *Health and Environmental Effects of Particulate Matter* in *EPA.gov*. 2016.

7. Weinmayr, G., et al., *Long-term exposure to fine particulate matter and incidence of type 2 diabetes mellitus in a cohort study: effects of total and traffic-specific air pollution.* Environ Health, 2015. **14**: p. 53.

8. Gladstein, N.A., *Ultrafine Particulate Matter and the Benefits of Reducing Particle Numbers in the United States*. 2013.

9. *Health and Environmental Effects of Particulate Matter* in *EPA.gov*. 2016.

10. Jacobson, M.Z., *Control of fossil-fuel particulate black carbon and organic matter, possibly the most effective method of slowing global warming.* Journal of Geophysical Research, 2002. **107**(D19).

11. Piock, W., et al., *Strategies Towards Meeting Future Particulate Matter Emission Requirements in Homogeneous Gasoline Direct Injection Engines.* SAE Int. J. Engines, 2011. **4**(1): p. 1455-1468.

12. Mamakos, A., et al., *Assessment of different technical options in reducing particle emissions from gasoline direct injection vehicles.* Journal of Aerosol Science, 2013. **63**: p. 115-125.

13. Brezny, R., *Particulate Control Experience with GDI and GPFs*, in *Manufacturers of Emission Controls Association*. 2016.

14. Barnes, C., *Effect of Ethanol on the Oxidative Reactivity of Gasoline Direct Injection Particulate*, in *Mechanical Engineering*. 2017, Texas A&M University.

15. Zhang, M., et al., *Influence of diluents on combustion and emission characteristics of a GDI engine.* Applied Thermal Engineering, 2017. **124**: p. 746-755.

16. Craig, A., et al., *Low Cost LEV-III, Tier-III Emission Solutions with Particulate Control using Advanced Catalysts and Substrates.* SAE International Journal of Engines, 2016. **9**(2): p. 1276-1288.

17. Saliba, G., et al., *Comparison of Gasoline Direct-Injection (GDI) and Port Fuel Injection (PFI) Vehicle Emissions: Emission Certification Standards, Cold-Start, Secondary Organic Aerosol Formation Potential, and Potential Climate Impacts.* Environmental Science & Technology, 2017. **51**(11): p. 6542-6552.

18. Chen, L., et al., *Characterizing particulate matter emissions from GDI and PFI vehicles under transient and cold start conditions.* Fuel, 2017. **189**: p. 131-140.

19. Zhu, R., et al., *Tailpipe emissions from gasoline direct injection (GDI) and port fuel injection (PFI) vehicles at both low and high ambient temperatures.* Environmental Pollution, 2016. **216**(Supplement C): p. 223-234.

20. Guan, B., et al., *Review of the state-of-the-art of exhaust particulate filter technology in internal combustion engines.* J Environ Manage, 2015. **154**: p. 225-58.

21. Merkel, G.A., et al., *Effects of Microstructure and Cell Geometry on Performance of Cordierite Diesel Particulate Filters*. 2001, SAE International.

22. Ogyu, K., et al., *Study on Filter Substrate Structure for Lower Backpressure and Higher Regeneration Performance*. 2006, SAE International.

23. Mokhri, M.A., et al., *Soot Filtration Recent Simulation Analysis in Diesel Particulate Filter (DPF).* Procedia Engineering, 2012. **41**: p. 1750-1755.

24. Petasch, J.A.U., *Effect of Membranes in Exhaust Particulate Filtration.* 40th Int'l Conference & Expo on Advanced Ceramics & Composites (ICACC 2016), 2013.

25. Konstandopoulos, A.G. and J.H. Johnson, *Wall-Flow Diesel Particulate Filters—Their Pressure Drop and Collection Efficiency*. 1989, SAE International.

26. Ohara, E., et al., *Filtration Behavior of Diesel Particulate Filters (1)*. 2007, SAE International.

27. White, J., *SIZE-DEPENDENT FILTRATION OF NON-LOADED PARTICULATE TRAPS*, in *Mechanical Engineering*. 2014, Texas A&M University.

28. Sheppard, J., P. Yang, and A. Strzelec, *Modeling and Experimentation of GDI-sized Particulate Filtration and Pressure-drop Behavior in Uncoated Commercial DPF Substrates.* Emission Control Science and Technology (Submitted), 2017.

29. Parks, J.E., et al., *Filter-based control of particulate matter from a lean gasoline direct injection engine*. 2016, SAE International.

30. Maricq, M.M., J.J. Szente, and K. Jahr, *The Impact of Ethanol Fuel Blends on PM Emissions from a Light-Duty GDI Vehicle.* Aerosol Science and Technology, 2012. **46**(5): p. 576-583.

31. Dalla Nora, M., T.D.M. Lanzanova, and H. Zhao, *Effects of valve timing, valve lift and exhaust backpressure on performance and gas exchanging of a two-stroke GDI engine with overhead valves.* Energy Conversion and Management, 2016. **123**: p. 71-83.

32. Watling, T.C., et al., *Development of a Particulate Filter Model for the Prediction of Backpressure: Improved Momentum Balance and Entrance and Exit Effect Equations.* SAE International Journal of Engines, 2017. **10**(4).

33. Hashimoto, S., et al., *SiC and Cordierite Diesel Particulate Filters Designed for Low Pressure Drop and Catalyzed, Uncatalyzed Systems*. 2002, SAE International.

34. Song, J., et al., *Fuel Sulfur Effect on Membrane Coated Diesel Particulate Filter*. 2002, SAE International.

35. Mizuno, Y., et al., *Study on Wall Pore Structure for Next Generation Diesel Particulate Filter*. 2008, SAE International.

36. Ogyu, K., et al., *Characterization of Thin Wall SiC-DPF*. 2003, SAE International.

37. Custer, N., et al., *Lubricant-Derived Ash Impact on Gasoline Particulate Filter Performance.* SAE International Journal of Engines, 2016. **9**(3): p. 1604-1614.

38. Wang, Y. and C. Kamp, *The Effects of Mid-Channel Ash Plug on DPF Pressure Drop*, in *SAE Technical Paper Series*. 2016.

39. Sappok, A. and V.W. Wong, *Ash Effects on Diesel Particulate Filter Pressure Drop Sensitivity to Soot and Implications for Regeneration Frequency and DPF Control.* SAE International Journal of Fuels and Lubricants, 2010. **3**(1): p. 380-396.

40. Lambert, C.K., et al., *Analysis of Ash in Low Mileage, Rapid Aged, and High Mileage Gasoline Exhaust Particle Filters.* SAE International Journal of Engines, 2017. **10**(4): p. 1595-1603.

41. Panu Karjalainen, L.P., Juha Heikkila, Tero Lahde, Theodoros Tzamkiozis, Leonidas Ntziachristos, Jorma Keskinen, Topi R€onkk€o, *Exhaust Particles of Modern Gasoline Vehicles: A Laboratory and an Onroad.* 2014,(97): p. 262-270.

42. Viswanathan, S., et al., *Experimental investigation of the effect of inlet particle properties on the capture efficiency in an exhaust particulate filter.* Journal of Aerosol Science, 2017. **113**: p. 250-264.